Response of Subdaily L-Band Backscatter to Internal and Surface Canopy Water Dynamics

Paul C. Vermunt, Saeed Khabbazan, Susan C. Steele-Dunne, *Member, IEEE*, Jasmeet Judge, *Senior Member, IEEE*, Alejandro Monsivais-Huertero, *Senior Member, IEEE*, Leila Guerriero, *Member, IEEE*, and Pang-Wei Liu, *Member, IEEE*

***Abstract*— The latest developments in radar mission concepts suggest that subdaily synthetic aperture radar will become available in the next decades. The goal of this study was to demonstrate the potential value of subdaily spaceborne radar for monitoring vegetation water dynamics, which is essential to understand the role of vegetation in the climate system. In particular, we aimed to quantify fluctuations of internal and surface canopy water (SCW) and understand their effect on subdaily patterns of L-band backscatter. An intensive field campaign was conducted in north-central Florida, USA, in 2018. A truck-mounted polarimetric L-band scatterometer was used to scan a sweet corn field multiple times per day, from sowing to harvest. SCW (dew, interception), soil moisture, and plant and soil hydraulics were monitored every 15 min. In addition, regular destructive sampling was conducted to measure seasonal and diurnal variations of internal vegetation water content. The results showed that backscatter was sensitive to both transient rainfall interception events, and slower daily cycles of internal canopy water and dew. On late-season days without rainfall, maximum diurnal backscatter variations of >2 dB due to internal and SCW were observed in all polarizations. These results demonstrate a potentially valuable application for the next generation of spaceborne radar missions.**

***Index Terms*— Backscatter, corn, dew, diurnal, ground-based, interception, L-band, sap flow, scatterometer, subdaily radar, vegetation, water content.**

I. Introduction

GLOBAL, daily to subdaily monitoring of vegetation water dynamics is essential to address fundamental questions surrounding the role of vegetation in the climate system, and to provide information for a range of applications from agriculture and water management to weather prediction [1]. Vegetation temporally stores water inside its tissue and on its surface, and this water is transferred back to the climate system through transpiration and evaporation. Global evapotranspiration (ETo) amounts from reanalysis data, land surface model, and diagnostic products disagree by up to 50% [2], [3], and trends are uncertain [4]. Uncertainty in ET partitioning is even more severe than uncertainty in estimating ET itself [5], [6]. Lack of understanding of rainfall interception by vegetation and its loss through evaporation is a key limitation of current methods to estimate and partition ET, and is essential for land surface modeling and understanding the role of vegetation in land–atmosphere interactions [7], [8]. Robust modeling of interception is hindered by holes in our basic process understanding [6], and a lack of information about surface canopy water (SCW), i.e., water storage on vegetation surfaces as a result of dew formation or intercepted precipitation [9]. Furthermore, there is a fundamental need for leaf wetness monitoring to understand how projected changes in climate will influence the timing, frequency, duration, and intensity of leaf wetting events and their effects on plant function in terms of water relations, gas exchange, energy balance, pathogens and pests, and reproduction [10].

A new perspective on ET and leaf wetness may be provided by subdaily synthetic aperture radar (SAR), which gives direct insight into the mass balance of the vegetation. Active microwave remote sensing has been found to be sensitive to canopy water storage, depending on frequency, polarization, incidence angle, and vegetation cover [11]–[17]. This sensitivity has mainly been studied to account for the confounding effect of vegetation on soil moisture retrieval, e.g., [18]–[20]. However, radar is also a valuable tool for vegetation monitoring, and well-suited to many applications including forest biomass and height [21], change detection [22], ecology and plant physiology [23], and agricultural crop classification and monitoring [24]. The launch of European Space Agency (ESA's) Sentinel-1 mission [25] in 2014 has accelerated the development of new applications for SAR in vegetation monitoring. By providing freely available data at an unprecedented high temporal resolution, Sentinel-1 has stimulated the rapid development of products for monitoring natural and agricultural landscapes. However, the repeat time of 6–12 days still limits the current state of the art to products related to biomass, leaf area index (LAI), phenological stage, change (e.g., harvest, tillage),

Manuscript received May 19, 2020; revised September 30, 2020; accepted October 31, 2020. This project was supported by Vidi Grant 14126 from the Dutch Technology Foundation STW, which is part of The Netherlands Organization for Scientific Research (NWO), and which is partly funded by the Ministry of Economic Affairs. *(Corresponding author: Paul C. Vermunt.)*

Paul C. Vermunt, Saeed Khabbazan, and Susan C. Steele-Dunne are with the Faculty of Civil Engineering and Geosciences, Delft University of Technology, 2628CN Delft, The Netherlands (e-mail: p.c.vermunt@tudelft.nl).

Jasmeet Judge is with the Department of Agricultural and Biological Engineering, University of Florida, Gainesville, FL 32611 USA.

Alejandro Monsivais-Huertero is with the Escuela Superior de Ingenieria Mecanica y Electrica Unidad Ticoman, Instituto Politecnico Nacional, Mexico City 07340, Mexico.

Leila Guerriero is with the Department of Civil Engineering and Computer Science, Tor Vergata University, 00133 Rome, Italy.

Pang-Wei Liu is with Hydrological Science Laboratory, NASA's Goddard Space Flight Center, Greenbelt, MD 20771 USA, and also with Science Systems and Applications, Inc., Lanham, MD 20706 USA.

Color versions of one or more figures in this article are available at https://doi.org/10.1109/TGRS.2020.3035881.

Digital Object Identifier 10.1109/TGRS.2020.3035881

and anomaly detection [26]–[31]. The Radarsat Constellation Mission (RCM) was launched in 2019, and consists of three identical SAR satellites. The resulting denser temporal sampling of RCM (4-day revisit time) compared to Radarsat-2 (12-day revisit time), is also expected to improve the potential of real-time agricultural monitoring with the Radarsat series [32].

The motivation for the current study is that the latest developments in radar mission concepts indicate that subdaily SAR data will become available in the next decades. CapellaSpace [33] and Iceye [34] are currently populating constellations of X-band (∼10 GHz) SAR systems in Low Earth Orbit (LEO), capable of delivering hourly data with resolutions of 10 m or less (e.g., [35]). An alternative is to place a SAR instrument in a geostationary orbit. A mission of particular interest is HydroTerra, one of the candidates bidding to become the ESA's 10th Pathfinder mission. HydroTerra is a C-band (∼5 GHz) geostationary (GEO) SAR mission which will deliver data at various spatial and temporal resolutions to meet the science needs of users [36]. L-band (∼1 GHz) geostationary SAR missions are also under development [37]. With Medium Earth Orbit (MEO) SAR, at altitudes between those of LEO and GEO, tradeoffs in system and orbit parameters allow a range of possibilities in terms of spatial and temporal resolution [38]. The goal of this study is to demonstrate the potential value of subdaily SAR to monitor internal and SCW, and exploit this emerging technology as a tool to address fundamental challenges in our understanding of the role of vegetation in the climate system.

Several studies have demonstrated that spaceborne radar is capable of detecting plant water variations during the day. Konings *et al.* [39], Paget *et al.* [40], and van Emmerik *et al.* [41] used aggregated data from the nonsun-synchronous RapidScat scatterometer (2014–2016) to demonstrate that the diurnal cycles in Ku-band radar backscatter were discernible over vegetated areas. Konings *et al.* [39] and Emmerik *et al.* [41] related variations in the daily cycle of Ku-band backscatter to vegetation water stress in the humid tropical forests of Central Africa and the Amazon, respectively. Other studies used aggregated data from scatterometers in sun-synchronous orbits to study diurnal variations in canopy water [42]–[45]. Frolking *et al.* [42] found Ku-band backscatter over the Amazonia to be up to 1.0 dB lower at 6:00 compared to 18:00. This difference decreased when a major regional drought continued. Schroeder *et al.* [43] and Friesen *et al.* [44] observed diurnal differences in C-band backscatter in the United States (∼10:00 and 22:30) and on a global scale (∼9:30 and 21:30), respectively. In a study on North-American grasslands, Steele-Dunne *et al.* [45] found mean differences between evening (21:30) and morning (9:30) observations of C-band backscatter between −0.6 and 0.6 dB, depending on region and season. The limitation of radar data from current satellites is that they are in sun-synchronous orbits, and data only available at fixed times (e.g., Advanced SCATterometer (ASCAT) at 10 am/10 pm). These times may not coincide with the ideal times to observe plant water variations, do not provide enough detail to capture and study daily cycles, and their data generally need to be aggregated to draw meaningful conclusions. The future availability of spaceborne subdaily SAR data therefore offers a unique possibility to study vegetation water dynamics at an unprecedented temporal resolution.

Ground-based radar experiments on subdaily variations in backscatter have a longer heritage, and have shown that radar backscatter is sensitive to vegetation water changes during the day. Using a truck-mounted dual-pol radar spectrometer scanning densely vegetated sorghum fields, Ulaby and Batlivala [46] combined 13 data acquisitions within ten days, where each acquisition was conducted at a different time of day. Aggregating these data, they found clear diurnal variations which they attributed to vegetation. Brisco *et al.* [16] used a truck-mounted Ku-, C-, and L-band quad-pol scatterometer to study subdaily fluctuations in backscatter measurements of a wheat canopy. They measured three full days, spread over two years. The results showed that for C- and L-band, the diurnal backscatter variation correlated well with measured vegetation water content (VWC) in the vegetative stage of the crop, while the correlation with soil moisture was higher when the plants were senescing. In addition, they showed that bulk VWC (including surface and internal water content) and HH-polarized C-band backscatter with 20° incidence angle in the vegetative stage of wheat following a diurnal cycle with maxima just after sunrise and minima between solar noon and sundown. Using results from the same experiment, Gillespie *et al.* [17] evaluated the effect of dew. The presence of dew was assessed by visual inspection, and backscatter patterns between two nights with and without dew were compared. They concluded that dew has an effect on C-band signals in particular, and that dew and internal canopy water effects can be differentiated according to timing and strength of response.

Other ground-based experiments focused on trees [47], [48]. Bouten *et al.* [47] measured the vertical attenuation profile of a Douglas fir stand before and after rain events. The X-band microwave generator and receiver were mounted on two towers, 12.5 m apart, and the beam of the transmitter was pointed in the direction of the receiver. They found a clear increase in attenuation after canopy wetting. Moreover, they estimated canopy surface water storage from precipitation and throughfall measurements and found high correlations with increments of the vertically integrated attenuation profiles. De Jong *et al.* [48] analyzed the relation between vertically polarized X-band backscatter and rainfall interception for a single ash tree. Backscatter observations during 14 rainstorms were averaged and compared to dry situations. The results showed a logarithmic increase of backscatter with cumulative precipitation, supported by physical model simulations. In addition, several studies have observed a diurnal cycle in trunk dielectric constant, which has been related to tree water status and sap flow [49]–[54].

These ground-based experiments successfully demonstrated that radar backscatter is sensitive to variations in total VWC. However, the limited data sets leave many open questions in terms of the sensitivity of radar backscatter to surface versus internal water content, the influence of phenological stage, and providing a quantitative link to water transport processes in the vegetation.

The aim of this study was to quantify fluctuations of internal and SCW and their effect on subdaily patterns of L-band backscatter with a view to demonstrating the potential value of subdaily spaceborne radar backscatter for monitoring vegetation water dynamics. An intensive field campaign was conducted over an entire growing season of corn, combining temporally dense radar backscatter observations with continuous observations of leaf surface wetness, surface and root zone soil moisture, sap flow, and meteorological variables, and frequent destructive vegetation sampling. These data were analyzed during the early-, mid- and late-season to study how backscatter in each polarization is affected by variations of internal and surface water content, and how this sensitivity varies as the crop develops. Data from the fully grown canopy were also combined to obtain an average daily cycle and insight into the influence of SCW on the amplitude and timing of the daily cycle of backscatter.

II. Materials and Methods

A. Study Site

The experiments were conducted in the spring of 2018 at the Plant Science Research and Education Unit (PSREU) of the University of Florida and the Institute of Food and Agricultural Sciences (UF—IFAS) at Citra, Florida (29.410N, 82.179W). Sweet corn (*Zea mays L. var. rugosa*) was sown in rows on April 13 and harvested on June 18. The average plant density was 7.9 plants m^{-2}. The soil at the field site consists of $>90\%$ sand [55], [56], which allows for high infiltration rates. Early in the growing season, the cornfield was irrigated several times with a center-pivot irrigation system. Irrigation was applied in the evening to minimize evaporative losses.

B. Radar Backscatter

Observations of the radar backscatter (σ^0) were made with the University of Florida L-band Automated Radar System (UF-LARS). A full description of the UF-LARS can be found in [57]. The UF-LARS operates at a center frequency of 1.25 GHz and is designed to collect horizontally (HH) and vertically (VV) co-polarized, and cross-polarized (HV and VH) combinations simultaneously. The system was mounted on a Genie manlift and scanned the cornfield with an antenna height of 14 m, and an incidence angle of 40°.

The backscatter coefficients are computed using the Single Target Calibration Technique (STCT) [58], [59]. To suppress fading, 27 independent samples are averaged [60]; nine samples were taken at 30 MHz increments from 1130–1370 MHz, for each of the three azimuthal scans at $-9°$, $0°$, and $+9°$. The total error was estimated by [60] to be 1.71 dB, and includes a systematic error of 1.49 dB and a random error of 0.85 dB (fading). The systematic error was estimated, via error propagation, by combining the measurement errors of calibration target geometry (1.4 dB), ranges between antenna to terrain (0.17 dB) and calibration target (0.35 dB), and incidence angle (0.32 dB) [57].

Ground range and azimuth resolutions were calculated based on the 3 dB beamwidth of 14.7° in the E-plane and 19.7° in the H-plane [57], and are provided in Table I.

TABLE I
Ground Range and Azimuth Resolutions

	range resolution (m)	azimuth resolution (m)
HH-pol	8.5	4.7
VV-pol	6.2	6.4
cross-pol	6.2	4.7

The resulting single-scan footprints in HH, VV, and cross-pol were 40.0, 39.7, and 29.1 m^2, respectively. Sampling areas (Section II-D) and *in situ* sensors (Section II-C) were located outside the arc swept by the radar, to avoid disturbing the scene.

For most of the season, 32 averaged σ^0 observations were obtained per day. For the last eight days of the season, the number of acquisitions was reduced to 16 to avoid radio frequency interference with other microwave sensors in the field. HV and VH polarizations were averaged and further shown as average cross-pol. All *in situ* sensors and vegetation sampling areas were located outside the footprint of the instrument.

C. Hydrometeorology

Meteorological data were obtained from the Florida Automated Weather Network (FAWN).[1] The 18-m tall FAWN weather station was located <600 m east from the experimental site. Observations of rainfall, the air temperature on 2 m height, solar radiation, relative humidity and wind speed are available every 15 min. Reference ETo was calculated from these data using an hourly version of the Penman-Monteith approach [61].

Sap flow is the flux of water through the plant, as water extracted by the roots is transported to the leaves to replenish water lost through transpiration. In large trees, the time lag between transpiration and sap flow measured at the base of a stem can be on the order of several hours, while the time lag between transpiration and sap flow at the crown is much smaller [62]–[64]. For corn, we observed that the time lag between calculated ETo and sap flow on the stem was on the order of minutes. Therefore, sap flow is a useful indicator of the timing and strength of the daily transpiration cycle which drives internal canopy water dynamics during the day.

Sap flow rates of four representative plants were measured with SGEX-19 Dynagage sap flow sensors (Dynamax Inc., Houston, TX, USA), which were installed close to other sensors, just outside the radar footprint. The measurements are based on the stem heat balance method [65]–[67]. Part of the lower stem tissue was continuously heated by external heater strips, and heat convection carried by the sap was measured. The sensors were enclosed by insulating and water-resisting materials, based on the method described in [68]. The built-in sap flow calculator of the Dynagage Flow32-1K system was used to estimate the sap flow rate [g h^{-1}] for each plant every 15 min. Sap flow [mm 15 min^{-1}] was calculated by averaging over the four sensors, converting the average weight

[1] https://fawn.ifas.ufl.edu/data/

of water to volume using the density of liquid water at 25 °C (0.997 g cm^{-3}), and multiplying the results for an "average" plant with the plant density. Because the installation of a SGEX-19 sensor requires a stem diameter of at least 15 mm, the sensors were first installed on May 18.

Data gaps, e.g., due to battery failure or poor contact, were filled using a linear relationship between sap flow and the transpiration component of Food and Agriculture Organization (FAO) crop ET (K_{cb}ETo) [69]. Here, ETo is the reference evapotranspiration, i.e. the ET from a hypothetical, well-watered grass reference surface, calculated using meteorological data from FAWN and the FAO Penman-Monteith method. K_{cb} is the basal crop coefficient for transpiration of a sweet corn canopy at potential rate. The multiplication with K_{cb} converts hypothetical ET of a grass surface into transpiration of a sweet corn canopy, assuming no limitation of water [69]. Linear regression between sap flow (F) and K_{cb}ETo was described by

$$F = 0.7222 \times K_{cb}\text{ETo} - 0.001 \tag{1}$$

with $R^2 = 0.871$, based on $n = 2389$ observations.

Leaf wetness due to dew and interception was monitored using three PYTHOS31 dielectric leaf wetness sensors (LWS). These sensors are designed to approximate the thermodynamic properties of leaves and output a voltage signal proportional to the dielectric of a 1 cm zone above the upper side of the sensor, which is proportional to the amount of water on the sensor [70]. This mV output is then converted automatically to a scale called "counts," to ensure that sensor outputs are universal regardless of the excitation voltage of the used data logger. For the EM50 data logger used here, counts = voltage(mV)/0.733 [70]. The sensors were attached to a wooden pole in between two rows in the early season. They were reattached to the corn plants once the stems were strong enough. The sensors were installed at different heights to capture the vertical distribution of water droplets in the canopy. The empirical model of Cobos [71] was used to estimate the mass of water (M_w) deposited on the sensor surface [g m^{-2}]

$$M_w = 1.54 \times \exp(5.8 \times 10^{-3} \times \text{counts}). \tag{2}$$

Estimation of the mass of water on the canopySCW was performed in two steps. First, regular measurements of leaf height, length, and width were conducted, and leaf areas were estimated by assuming that corn leaves have an elliptical shape with the assumption that corn leaves approximate the shape of an ellipse

$$A_{\text{leaf}} = \pi \times l \times \frac{w}{4} \tag{3}$$

where A_{leaf} is the leaf area [m^{-2}], l is leaf length [m], and w is leaf width [m]. Second, it was assumed that the wetness of a leaf at any height could be approximated as that of the nearest sensor

$$\text{SCW} = \rho_{\text{plant}} \times \sum_{i=1}^{n} A_{\text{leaf}i} \times M_{wi} \tag{4}$$

where SCW is SCW per square meter of ground [kg m^{-2}], ρ_{plant} is the average number of plants per m^{-2}, M_{wi} is the water mass on the sensor closest to leaf i [kg m^{-2}], and n is the number of leaves per plant.

Root zone soil moisture was measured with ten Decagon EC-5 sensors, which were installed in two pits at five different depths: 5, 10, 20, 40, and 80 cm. The pits were located 40 m apart but centered between the same two rows. Site-specific calibration was performed yielding a linear regression R^2 of 0.993. Soil moisture was similar in both pits. Hence, the presented results are the averages over the two pits. Linear interpolation between the measurements was applied to visualize root zone soil moisture.

Soil water potential was monitored using two T4e pressure transducer tensiometers [72]. These were installed 40 m apart, close to the soil moisture pits. The centers of the ceramic cups were located at a depth of 20 cm. The presented results are the averaged signals of both tensiometers.

D. Vegetation Sampling and Monitoring

VWC and dry biomass (m_d) were measured using destructive sampling. Four sampling areas were established outside the arc swept by the radar, and outside the *in situ* sensor locations, at the beginning of the season. Each sampling time, two representative samples were taken from each of these four sampling areas. Any surface water present on the plant tissue was removed with a paper towel before weighing. From the eight samples, the stems, leaves, tillers, tassels, and ears were separated, weighed, and oven-dried on 60 °C for 4–5 days in the early season to 7 days in late season. The dry samples were weighed again, and VWC [kg m^{-2}] was derived from (5)

$$\text{VWC} = (m_f - m_d)\rho_{\text{plant}} \tag{5}$$

where m_f is the average fresh weight or fresh biomass of the eight samples [kg], m_d is the average dry weight or dry biomass of the eight samples [kg], and ρ_{plant} is the number of plants per square meter of ground. Gravimetric water content, M_g, is the mass of water per unit mass of fresh biomass ((6))

$$M_g = \frac{m_f - m_d}{m_f}. \tag{6}$$

Equations (5) and (6) were applied for each of the plant constituents (i.e., leaves, stems, tillers, and ears) separately.

Sampling was conducted before sunrise (6 am) to minimize the effect of transpiration on the measurements that represent the seasonal variability of VWC and M_g. These predawn measurements were scheduled three times per week. On one of these three days, one extra sampling was performed during the day in order to capture diurnal variations. This second sampling was at 6 pm, which would be the time of the corresponding evening pass for a sun-synchronous satellite such as SMAP [73].

Plant growth stages were visually identified three times per week, using the *Biologische Bundesanstalt, Bundessortenamt, and Chemical industry* (BBCH) scale for corn [74]. The cut samples were used to measure plant heights. LAI was calculated by multiplying the averaged, estimated leaf areas by plant density.

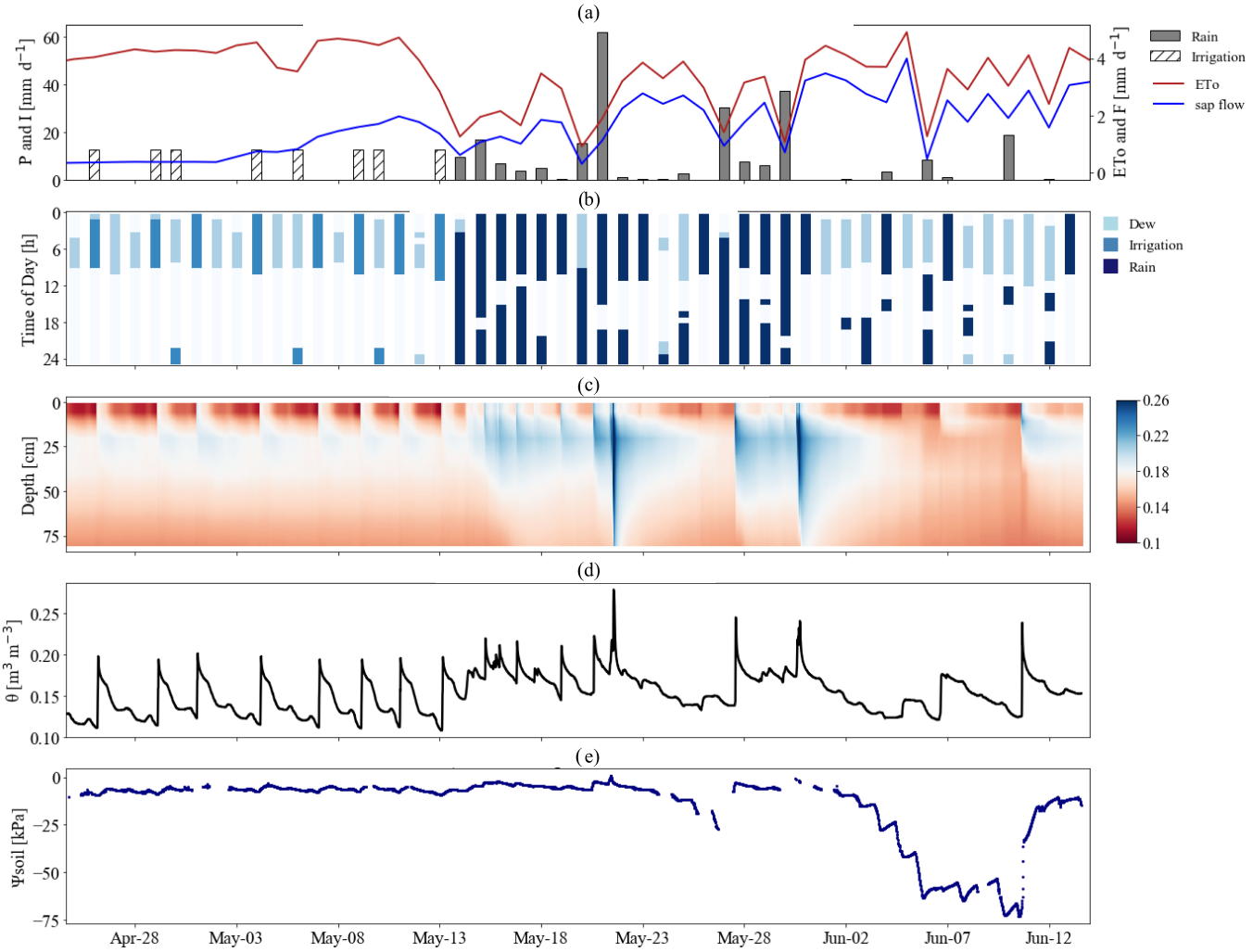

Fig. 1. Time series of (a) rainfall, irrigation, and ETo, (b) presence of SCW resulted from dew, irrigation, or rain, (c) volumetric root zone soil moisture content, (d) surface soil moisture content only, and (e) soil water potential at 20 cm depth.

III. Results

A. Hydrometeorology

Fig. 1 shows the hydrometeorological and soil moisture conditions during the growing season. The first three weeks of the season were characterized by high levels of ETo and an absence of precipitation [Fig. 1(a)]. On several days, midnight irrigation was applied to control soil moisture content [Fig. 1(a)–(d)], leading to a soil water potential which is favorable for root water extraction as soon as the roots reach deep enough [Fig. 1(e)]. These conditions allowed for high rates of transpiration. Water films on leaf surfaces were detected every morning [Fig. 1(b)] as a result of dew formation, interception of sprinkler irrigation, or a combination of both, and disappeared at around 10:00 every morning.

The mid-season weather conditions featured frequent, tropical rainfall and thunderstorms [Fig. 1(a)]. This resulted in water droplets on the canopy for long periods during the day [Fig. 1(b)], and several sharp increases in root zone soil moisture content [Fig. 1(c)]. Limited rain between May 22 and 27 led to a temporary reduction in root zone soil moisture content and potential [Fig. 1(d) and (e)].

A dry period with high temperatures and solar radiation started on June 1. This produced high evaporative demand [ETo in Fig. 1(a)], which resulted in a rapid decrease of soil moisture in the root zone. Despite the limited root zone soil moisture, leaf surfaces were wet every morning, mainly because of dew formation [Fig. 1(b)]. A substantial rain event on June 10 ended the dry period.

B. Vegetation Development and Water Content

The sweet corn crop development is illustrated in Fig. 2. Corresponding explanations of the BBCH phenology codes can be seen in Table II. Fig. 2(a) shows the plant height and dry biomass accumulation [kg m^{-2}] of the total plant and individual plant constituents during the life cycle, based on destructive vegetation sampling data. Fig. 2(b) and (c) shows how the water content of the plant and its constituents vary during the growing cycle. Fig. 2(b) shows the mass of water stored in [kg m^{-2}], a measure commonly used in microwave remote sensing. Fig. 2(c) shows this water storage in terms of gravimetric moisture content, which is the mass of water per total mass of the plant. This is more closely related to the relative water content used by plant physiologists.

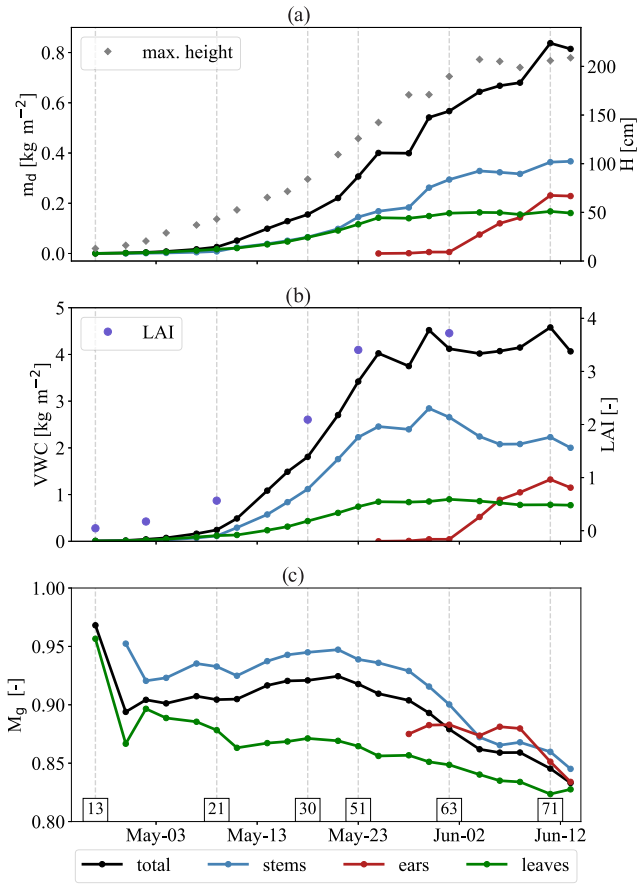

Fig. 2. Seasonal patterns of (a) dry biomass and maximum canopy height, (b) predawn VWC and LAI, and (c) predawn gravimetric water content, including the contributions of dominant plant constituents to total. Important phenological stages are represented by BBCH codes, which are explained in Table II.

TABLE II
CROP DEVELOPMENT STAGES

BBCH	Stage of development	Dates
13	Leaf development – 3 leaves (V)	Apr 25
21	Start of tiller formation (V)	May 7
30	Start of stem elongation (V)	May 18
51	Start of tassel emergence (V)	May 23
63	Male: start pollen shedding.	Jun 1
	Female: stigmata tips visible (R)	
71	Start of grain development:	Jun 11
	kernels at blister stage (R)	

V=vegetative stage. R= reproductive stage.

First plant emergence was observed on April 19, six days after sowing. Although leaf and stem dry biomass (m_d) increased at similar rates until plants reached half their final height [Fig. 2(a)], stems held substantially more water [Fig. 2(b) and (c)]. At the end of the vegetative stage, 65% of all VWC was stored in the stems.

In the reproductive stage, ear formation coincided with VWC decreases in all other constituents, especially in the stems. From May 30 to June 6, water storage in the stems decreased by almost 30%: -0.8 kg m^{-2}, as the ears formed

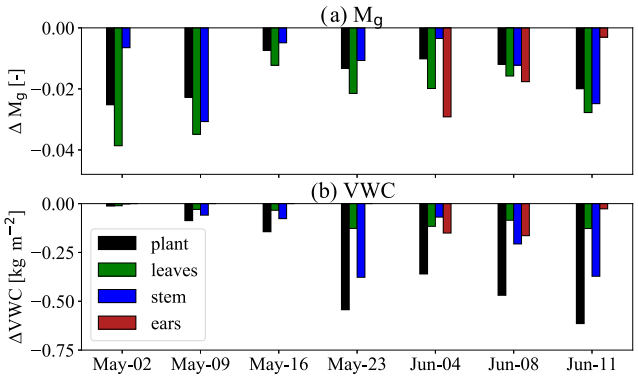

Fig. 3. Change (6:00 minus 18:00) in internal canopy water content of total plant and dominant constituents, represented as (a) gravimetric moisture loss and (b) equivalent weight of moisture loss [kg m^{-2}].

and separated from the main stem [Fig. 2(b)]. Leaf senescence of the lowest leaves occurred from June 2 onward. The reproductive stage largely coincided with the dry period shown in Fig. 1. The corn was harvested five days after the last sampling.

The results of the seven days of twice-daily destructive vegetation sampling are shown in Fig. 3. The figure shows the internal canopy water differences between 6:00 and 18:00 for the total plant and the most important constituents (by biomass). The smallest $\Delta\ M_g$ was observed on May 16, when cloud and rain limited transpiration. Significant decreases in internal water content were observed in the early season, as a result of high atmospheric demand for ET [Fig. 1(a)], a shallow root zone, and a relatively dry upper soil [Fig. 1(c)]. These differences in M_g translate to small ΔVWC [Fig. 3(b)] due to the limited fresh biomass in the early vegetative stages. In the reproductive stage, diurnal moisture losses in stems increased, while such losses decreased for ears. At this stage, ears grow and store water, while the internal water content of the stems starts to decrease. These subdaily variations were substantial compared to the seasonal predawn M_g variations [Fig. 2(c)]. It should be noted that maximum subdaily moisture variations may be higher than the difference between 6:00 and 18:00.

C. Backscatter

1) Seasonal Variations in Backscatter: Backscatter coefficients (VV, HH, and average cross-pol) are shown in Fig. 4. Backscatter increased in all polarizations with the growth of the crop. Copolarized backscatter increased from <-14 dB after planting to about -5 dB when plants reached half of their total biomass, while cross-polarized backscatter increased from <-32 dB to about -16 dB.

The influence of early season irrigation events (Fig. 1) is apparent in all polarizations (Fig. 4). Sensitivity to wetting events (irrigation and rainfall) decreased as the canopy grew and σ^0 became increasingly sensitive to wet biomass (Appendix).

The increasing trend in σ^0 due to vegetation growth tapers off around May 20. These high values, 3–4 days prior to plant VWC and LAI maxima can be explained by the heavy rainstorms around May 20. Precipitation from these storms

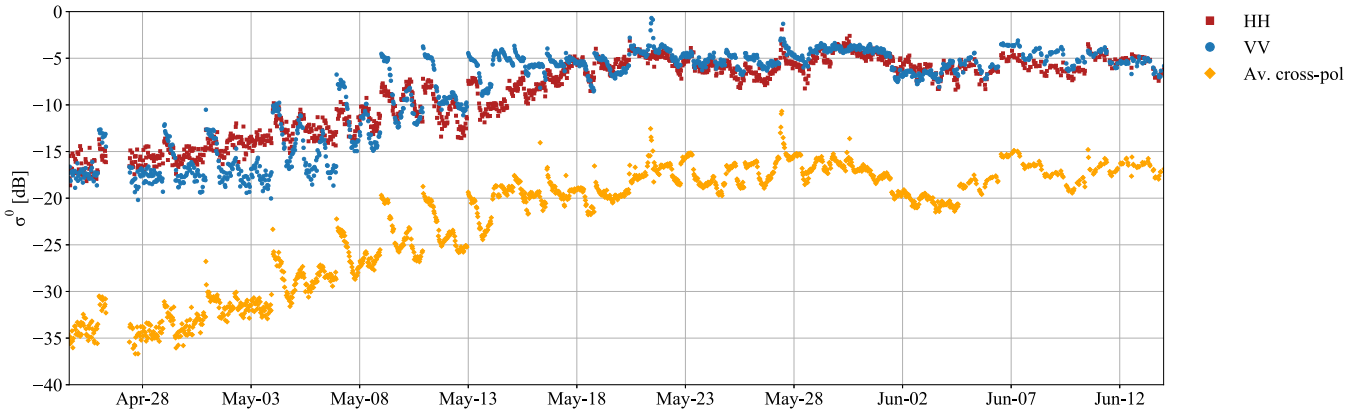

Fig. 4. Time series of observed L-band co- and cross-polarized backscatter.

increased both canopy surface wetness and soil moisture, which produced high σ^0 values in all polarizations. Nonetheless, responses to some events after this date were observed. The decrease in σ^0 from June 1 corresponds with the drop in soil moisture (Fig. 1) and the sharp reduction in stem water content [Fig. 2(b)]. Backscatter increased again following small rain events and the formation and separation of ears.

2) Early Season: Two three-day periods in the early season are highlighted in Fig. 5. Fig. 5(a)–(c) shows a period of 11–13 days after emergence when bare soil exposure was still considerable and plant height was just 15–20 cm. Fig. 5(a) shows co- and cross-polarized backscatter. Fig. 5(b) shows raw data counts from two LWSs positioned 7 cm above the ground, as well as the sap flow. Fig. 5(c) shows the precipitation at the nearby weather station and the soil moisture observed at 5 cm depth. The irrigation event on April 30 lead to an increase in soil moisture at 5 cm depth, and a sharp increase in σ^0 of up to 5 dB. Clear cyclic variations of 2–3 dB are observed in σ^0, particularly in σ_{VV}. These cannot be explained by the 5 cm soil moisture, but seem to follow the accumulation and dissipation of dew on the vegetation and soil surface as indicated by LWS data in Fig. 5(b). The LWS counts increase during the night as dew accumulates on the sensor. The LWS counts decrease rapidly after sunrise as the increase in solar radiation allows the dew to evaporate. On each of the days shown in Fig. 5, and also in Fig. 1(b), the dew has generally dissipated by 10:00 am. It is important to note that, in addition to forming on the leaves and the LWS, dew also forms as a film of water on the soil surface. It is clear from Fig. 5(c) that it is insufficient to infiltrate the soil and reach the sensor at 5 cm. However, L-band backscatter is dominated by surface scattering from the soil at this stage ([75]–[78], and Fig. 10), and the difference between a wet (e.g., 0.3 cm^3cm^{-3}) and dry (e.g., 0.1 $^3cm^{-3}$) soil can produce differences of up to 3.5 (HH) and 6 (VV) dB [79]. We postulate, therefore, that the accumulation and dissipation of this film of water on the soil surface is the most important reason behind the cyclic σ^0 variations in Fig. 5(a). The effect of dew on the topsoil is also clear in VV where the irrigation event on April 30 increases σ_{VV} from −18 dB to −13 dB, a value at which it stays due to the presence of dew until sunrise the following morning. Moreover, σ_{VV} ramps up as dew accumulates in the early hours of May 2, before decreasing again at sunrise.

Fig. 5(d)–(f) shows the measurements of one week later when the maximum plant height has increased to 37 cm (May 7) and 43 cm (May 9), LAI is around 0.57 and VWC is increasing from 0.16 kg m^{-2} (May 7) to 0.23 kg m^{-2} (May 9). While soil moisture values are comparable to those observed the week before, the σ^0 values in Fig. 5(d) are around 4 dB higher than those in Fig. 5(a) in all polarizations. From Fig. 10, this can be attributed to the increase in vegetation scattering in all polarizations, an increase in double-bounce in VV, and an increase in vegetation ground scattering in HH and cross-pol. In other words, the backscatter is increasing due to plant growth, and microwave interactions with vegetation are becoming increasingly important. Sap flow values are higher than in Fig. 5(b) due to an increase in the plant area and transpiration. The LWS has been repositioned at 10 and 20 cm to accommodate the growing plant, and a sensor was added at 30 cm on May 7.

Irrigation events on May 6 and 9 lead to sharp increases in soil moisture and σ^0. Increases of 8 dB (VV), 4 dB (HH), and 5–6 dB (cross-pol) were observed in response to the event on May 9. On May 7 and 9, initial rapid increases in LWS counts due to interception of irrigation were followed by more gradual increases as dew accumulated during the night. Steady dew accumulation is also observed during the night of May 7 and 8. On all three days, the accumulated moisture dissipated quickly after sunrise. The cyclic variations in σ^0 are clearer than they were in Fig. 5, and their correspondence with the LWS data is even more striking. The σ_{VV} is particularly responsive to the presence of water on the soil and vegetation. This may be due to the important role of double-bounce in σ_{VV} at this time.

3) Mid-Season: Fig. 6 shows two periods in the mid-season. Note that average σ^0 increased significantly since the early season, as a result of plant growth. In the time period shown in Fig. 6(a)–(c), the corn had started to tassel, and leaves had almost reached final sizes (Fig. 2). Fig. 10 shows that, for this growth stage, σ^0 is dominated by vegetation scattering. There are limited contributions from double-bounce in VV and HH, and the vegetation-ground term in HH. This is consistent with earlier research [75]–[78].

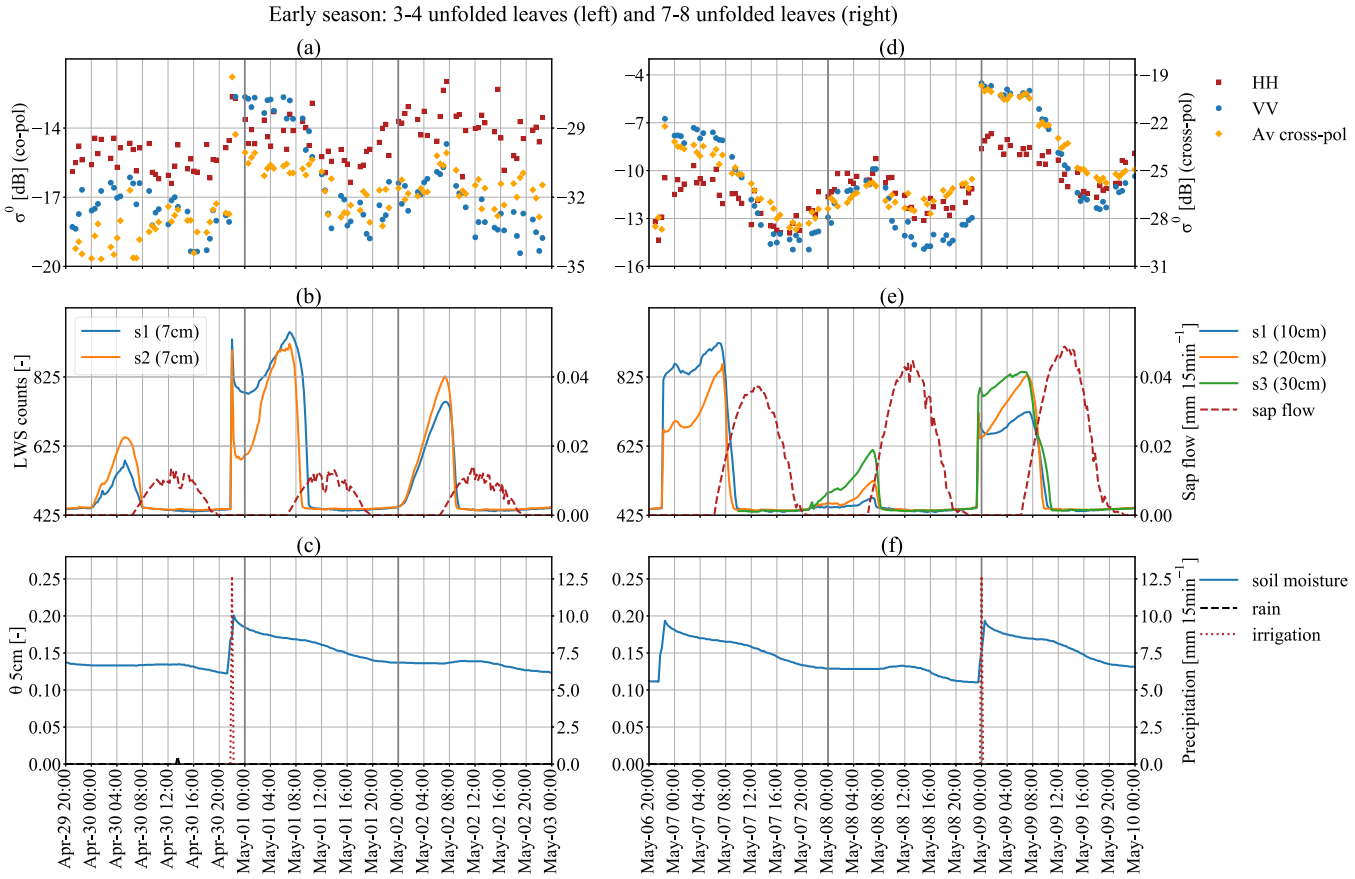

Fig. 5. Early season patterns of (a) and (d) co- and cross-polarization backscatter, (b) and (e) raw data counts from the LWSs and sap flow, and (c) and (f) surface soil moisture and precipitation. The left figures (a), (b), and (c) shows a 3-day period when plants reach 15–20 cm, while the right figures (d), (e), and (f) shows a 3-day period when plants reach 43–65 cm. Note that the vertical axes of the left and right backscatter plots are different.

Low-intensity rain events on May 23, 24, and 25 were intercepted by the almost fully grown leaves and had a negligible impact on soil moisture. This suggests that σ^0 variations in Fig. 6(a) can be attributed to variations in SCW and internal VWC [Fig. 6(a) and (b)]. Cross-pol backscatter, which is sensitive to leaf moisture content, increased rapidly in response to interception in the evenings of May 24 and 25. The presence of dew in the early hours of May 23 and 25, and an interception on May 24 and 25 resulted in elevated values of σ_{cross}. Rapid dissipation of dew in the early morning on May 23 and 25 produced a $\sim$2 dB drop in σ_{cross}. The difference in response of the three polarizations to SCW is particularly noticeable during the interception and dew events early on May 25, and could be explained by their relative sensitivities to different canopy constituents. Note that estimated interception sometimes exceeds measured rainfall. This could be due to 1) the simplistic model used to convert sensor output to full canopy interception (see Section II-C); 2) spatial rainfall variability (rainfall was collected 600 m from the studied field); 3) accuracy of rainfall data ($\sim$0.25 mm); or 4) spatial heterogeneity of interception itself due to e.g., variations in plant architecture.

Backscatter in all polarizations reflects variations in internal water content. Recall from Fig. 3 that internal water losses were high in this period ($\sim$0.5 kg m^{-2}) because of a relatively high atmospheric water demand (Fig. 1). The rise in sap flow and transpiration resulted in a decrease in σ^0, and water uptake in the evening resulted in an increase.

Fig. 6(d)–(f) illustrates the observations of one week later, after a four-day period of heavy rainfall (Fig. 1). The last rain event on May 30 was followed by two dry and hot days, resulting in a decrease in surface soil moisture. The limited variation in σ_{VV} and σ_{HH} in response to the sharp increases in SCW and soil moisture suggests that copol backscatter saturated at ~ -4 dB. Despite high rates of sap flow on May 31, diurnal cycles of σ_{VV} and σ_{HH} were not observed. This saturation was probably caused by a combination of a wet field (Fig. 1) and a peak in VWC (Fig. 2). May 31 was characterized by high ET rates, causing canopy surface water to disappear, and soil moisture to decrease. Meanwhile, stem water content started to drop significantly (Fig. 2). These losses of water led to a decrease in copol backscatter, which resulted in observed diurnal cycles of σ^0 again [Fig. 6(d)]. Dips in cross-polarized backscatter (May 31) and all polarizations (June 1) coincide with the dissipation of dew and peaks of sap flow.

4) Late Season: Fig. 7 shows observations from two periods in the late season during which the corn plants experienced the lowest root zone water availability of the season [Fig. 1(c) and (e)]. Recall from Fig. 3 that diurnal water fluctuations in response to transpiration during these days

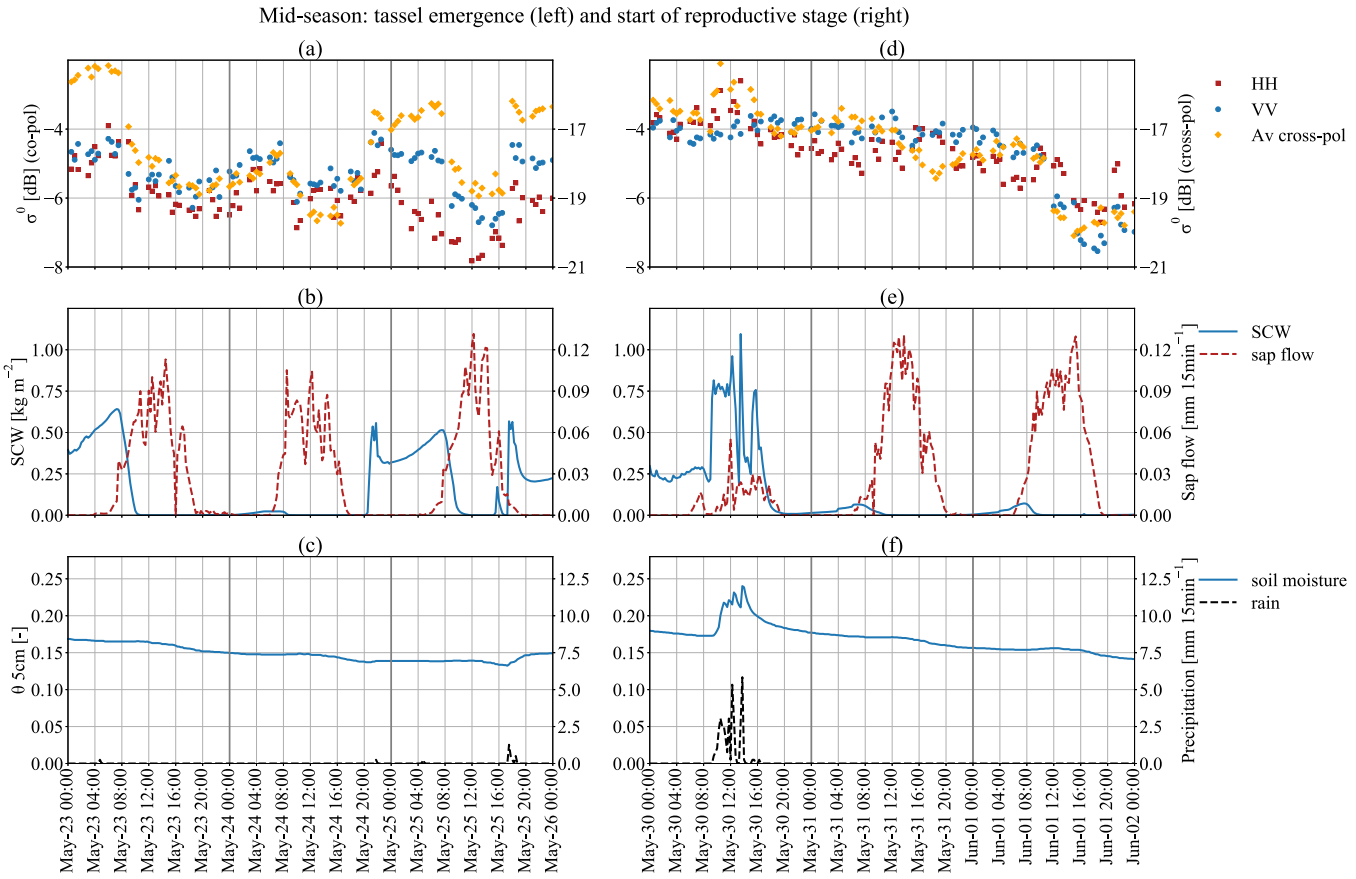

Fig. 6. Mid-season patterns of (a) and (d) co- and cross-polarization backscatter, (b) and (e) SCW and sap flow, and (c) and (f) surface soil moisture and precipitation. The left column (a), (b), and (c) shows a 3-day period when plants reach 125–140 cm, while the right column (d), (e), and (f) shows a 3-day period when plants reach 180–189 cm. Note that the vertical axes of backscatter and SCW are different from Fig. 5.

were considerable. Nonetheless, the plants were able to recover from water losses after solar noon; predawn M_g did not decrease with higher rates than in the wet period before (Fig. 2). Simulations in Fig. 10 suggest that σ_{cross} and σ_{VV} were dominated by vegetation scattering, while σ_{HH} still had limited sensitivity to ground-related terms.

The diurnal VWC cycles were discernible in σ^0 in all polarizations, particularly on the days without rainfall. On June 5, there is a noteworthy decrease of almost 4 dB in all polarizations. This coincides with a significant loss of internal water content (Fig. 3) due to transpiration [sap flow in Fig. 7(b)]. The minimal change in soil moisture at this time, and the fact that the decrease is consistent across polarizations suggests that this is a decrease in vegetation scattering due to the observed drop in internal water content. From midnight on June 9 to noon on June 10, soil moisture barely changes. Backscatter on the other hand, especially VV and cross-pol, increases with dew accumulation during the night and decreases as dew dissipates and transpiration leads to internal water content losses during the day. A similar response is observed in the response to dew and transpiration in the early hours of June 11. Again, the minimal variation in soil moisture and the consistency across polarizations suggest that this is a response to internal and SCW dynamics rather than sensitivity to soil moisture.

Precipitation events on June 4, 6, and 10 [Fig. 7(c) and (f)] resulted in spikes in interception [SCW in Fig. 7(b) and (e)]. The precipitation event of June 10 led to a substantial and prolonged increase of soil moisture. The limited effect this prolonged increase had on backscatter (particularly σ_{VV} and σ_{cross}) confirms the strong reduction to soil moisture sensitivity at this stage. Given the lack of sensitivity to surface soil moisture in VV and cross-pol, it is likely that these backscatter increases are primarily in response to interception rather than moisture on the soil surface.

5) Mean Daily Cycles: Figs. 5–7 show that subdaily variations in σ^0 included rapid variations due to the interception of intermittent precipitation events, and slower variations due to dew formation and dissipation and internal water content variations. To minimize the influence of random individual precipitation events and gain some insight into the average daily cycle, data were averaged over a 21-day period between May 23 and the last day of the experiment, June 13. This is the period in which σ^0 did not increase anymore as a result of crop growth (Fig. 4). Previous studies and model simulations suggest that the effect of soil moisture on σ^0 in all polarizations is limited in this period (Fig. 10, [75], [76], [78]).

Fig. 8 shows the mean diurnal cycle of σ^0, SCW and sap flow, soil moisture, and precipitation over this period.

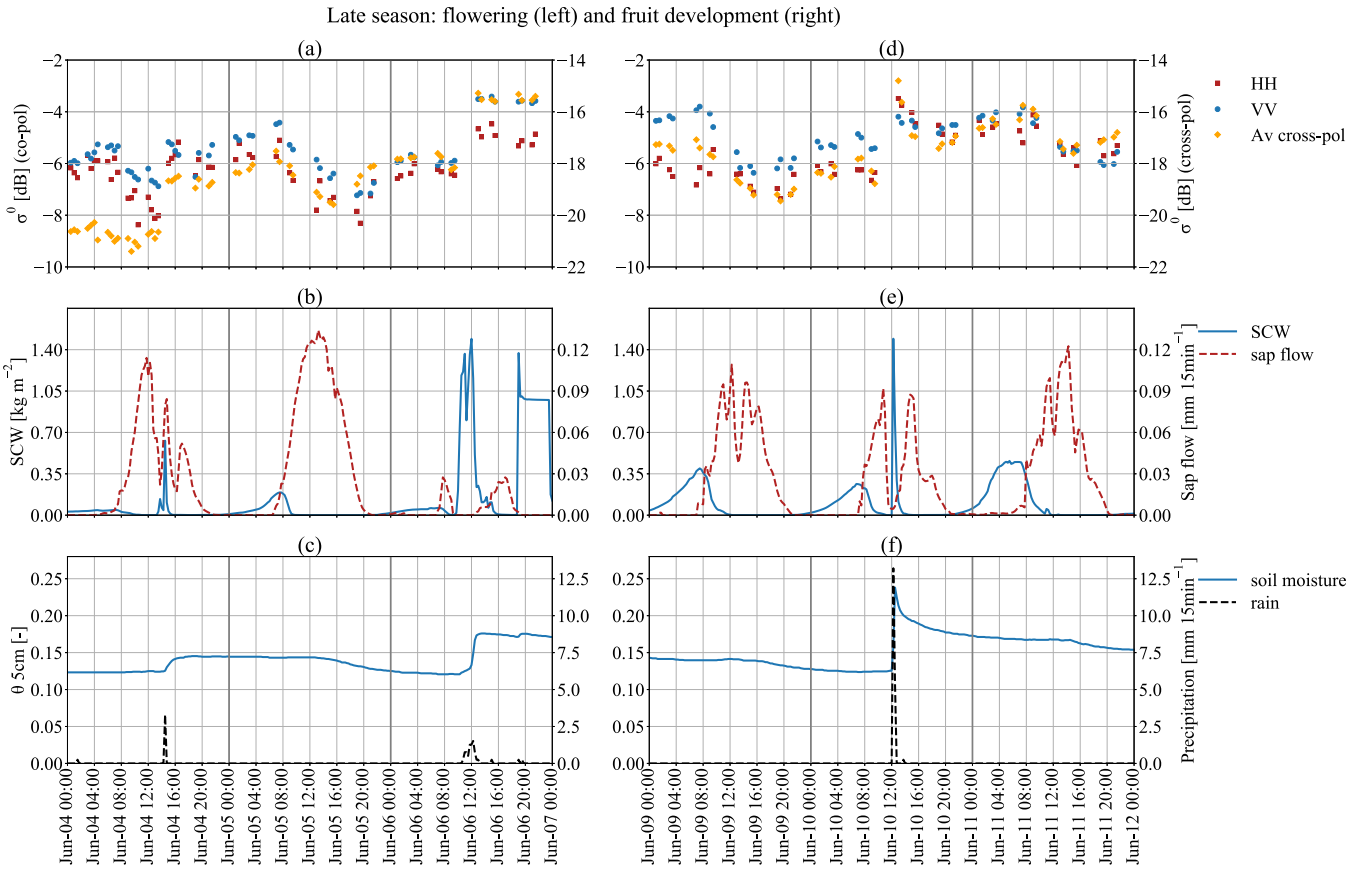

Fig. 7. Late season patterns of (a) and (d) co- and cross-polarization backscatter, (b) and (e) SCW and sap flow, and (c) and (f) surface soil moisture and precipitation. Maximum canopy height was stabilized at 205 cm during this period. Note that the temporal density of backscatter is less than in previous figures.

Clear daily cycles can be observed in σ^0, sap flow, and SCW. Peaks of VV and cross-pol coincide with the peak in SCW, and the start of the sap flow/transpiration cycle. After sunrise, the increase in net radiation drove transpiration and led to the dissipation of dew from the canopy. Backscatter dropped on average with 0.7 dB (VV), 0.6 dB (HH), and 1.0 dB (cross-pol) between sunrise and 15:00. After 15:00, there is a downward trend in sap flow and an upward trend in σ^0. Most rainfall events occurred during the daytime and they explain the fluctuations in averaged SCW during the afternoon. The peak values in rainfall at 09:45 and 12:15 were due to two major convective rainfall events, each of which resulted in a significant increase in average soil moisture but only a modest and transient effect on average SCW and σ^0.

To exclude the effect of rainfall completely, the four days without any rainfall within this period were plotted separately in Fig. 9. Note that there was a decreasing trend in σ^0 during this period due to the loss of internal water content of the stems in this growth stage, and the limited root zone soil moisture availability between June 5 and 9. Also note that sap flow was high in this period, so high subdaily variations of internal water content are expected. Temporal patterns were similar to those in Fig. 8, although the timing of the σ^0 minima is slightly different. Cross-polarized backscatter changed inflection again after the peak hours of ET, while VV-polarized backscatter changed inflection with the start of dew formation. In both Figs. 8 and 9, nocturnal increase is only observed in σ_{VV} and σ_{cross}. In the absence of precipitation, the average diurnal difference in σ^0 on these four days was 2.4 dB (VV), 1.6 dB (HH) and 2.0 dB (cross-pol).

IV. Discussion

Consistent with previous studies (e.g., [80]), L-band sensitivity to scattering from vegetation correlated with the buildup of VWC during the season (Fig. 2). With low vegetation, early season σ^0 patterns in all polarizations were consistent with soil moisture responses to wetting events (irrigation, precipitation), and even showed strong similarities with dew deposition on the topsoil (Fig. 5). Similar wetting events, with similar soil moisture responses, showed a much smaller effect on σ^0 in all polarizations in mid and late season (Figs. 4 and 7). In mid and late season, and particularly beyond May 18, differences between σ_{VV} and σ_{HH} were minimal. This can only be explained by the predominance of volume scattering, i.e., direct vegetation scattering, since stem attenuation and scattering, as well as double bounce is polarization-dependent [81]. This predominance of vegetation scattering is confirmed by the physical model simulations in Appendix and Fig. 10. Although it is not a persistent contribution, double bounce can still cause some sensitivity to soil moisture at HH polarization until the end of the season.

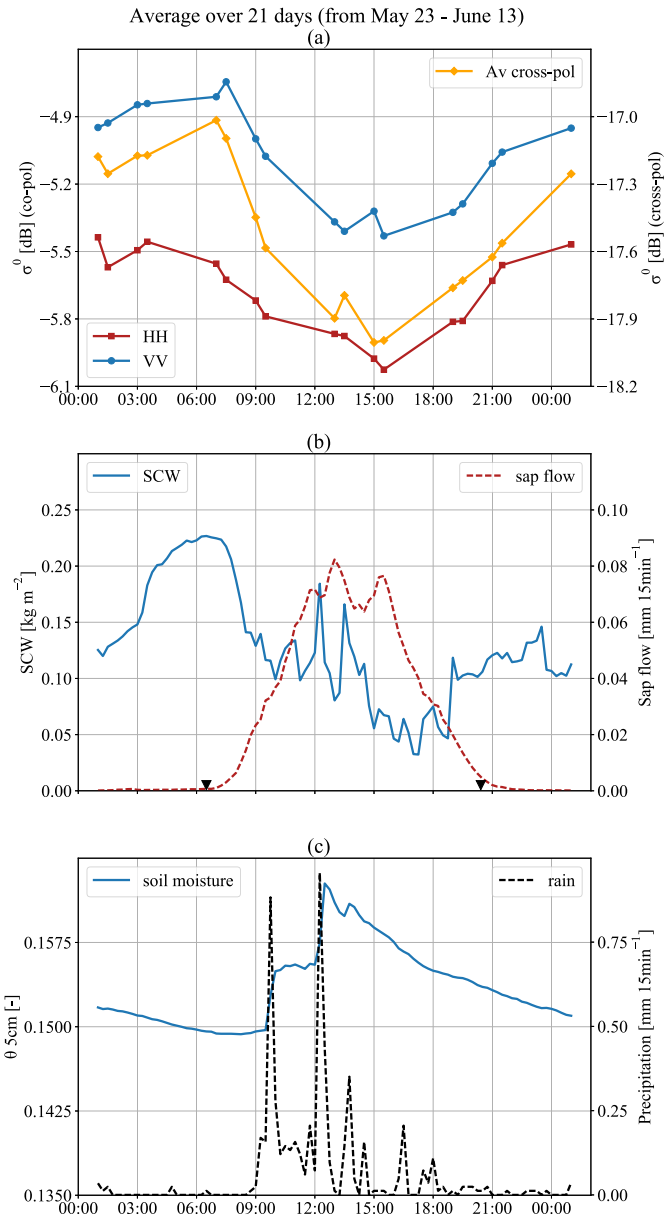

Fig. 8. Mean daily cycles of (a) co- and cross-polarized backscatter, (b) SCW and transpiration, and (c) soil moisture and rainfall, for the last 21-days of the season. Timing of sunrise and sunset are depicted with triangles in (b).

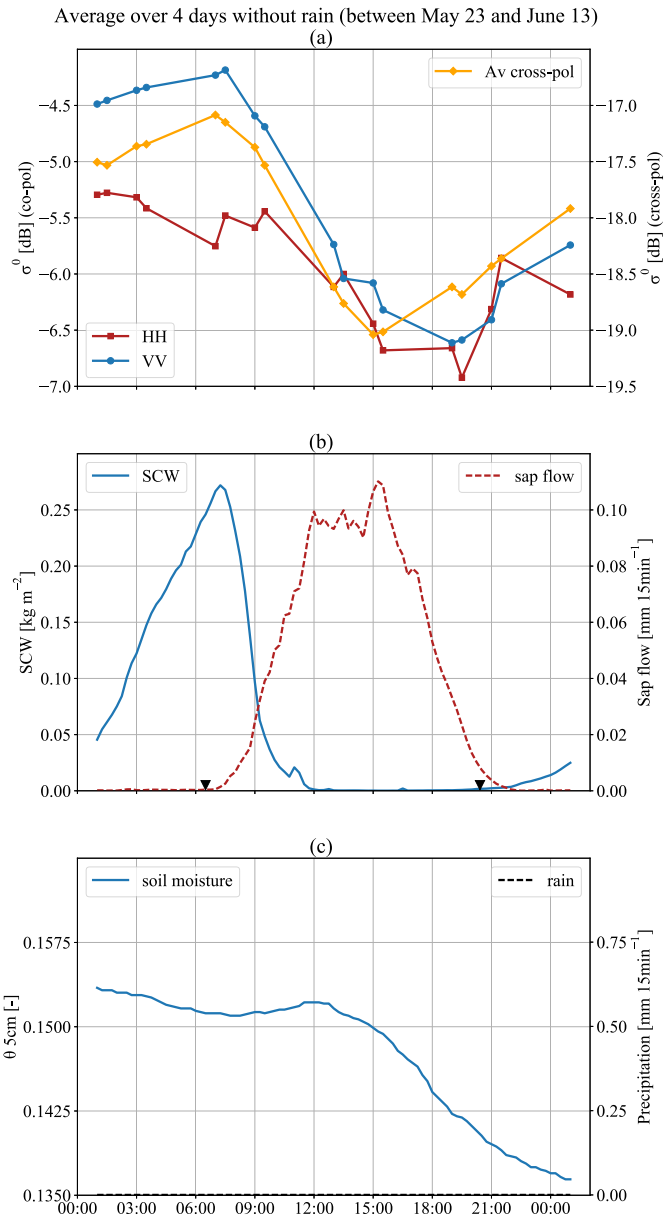

Fig. 9. Mean daily cycles of (a) co- and cross-polarized backscatter, (b) SCW and transpiration, and (c) soil moisture and rainfall, for only the four dry days within the last 21-days of the season. Timing of sunrise and sunset are depicted with triangles in (b).

The seasonal increased sensitivity to vegetation and reduced sensitivity to soil confirms previous work on L-band (e.g., [20], [75], [80]).

Subdaily backscatter variability has been attributed to variations in VWC in several studies (e.g., [39], [41], [82]). However, these satellite-based studies lacked ground validation data. The unprecedented destructive sampling data presented in this study confirm that subdaily variations in VWC are substantial (>0.5 kg m^{-2}, Fig. 3) even though corn is an isohydric species (i.e., water content is regulated through active stomatal control). This motivates further research to include other species.

The deepest drops in σ^0 were observed after the acquisition at 9:30, when dew almost dissipated completely (Fig. 9). This is also observed on dry days in Figs. 6 and 7. Since transpiration rates become substantial after this time, this suggests that diurnal VWC fluctuations govern the most substantial part of the subdaily σ^0 cycles in mid- and late season.

Several studies have attributed differences in diurnal backscatter to the presence of dew, but did not account for variations in internal VWC (e.g., [83]–[85]). The combination of intensive destructive vegetation sampling, continuous leaf wetness monitoring,, and high-revisit backscatter provides unique insight into their combined influence on the dynamics of subdaily backscatter and how that varies throughout the season. Gillespie *et al.* [17] provided one of the few studies in which both internal and surface water are considered in the context of dew detection. They found that the C-band HH-pol backscatter on a night without dew had a peak 1.5 h after

sunrise, corresponding to the peak in their observations of internal VWC [17]. On the other hand, the backscatter peak on a night with dew was at sunrise, which is the moment beyond dew starts to disappear. Similarly, our L-band observations show a subdaily backscatter maximum around sunrise, particularly in VV and cross-pol (Figs. 8 and 9). This is consistent with the peaks of dew accumulation and suggests that dew can have a significant effect on the timing and magnitude of the maximum of the subdaily backscatter cycle. While [17] provided the first indication that dew formation and dissipation determines the peak of (C-band, HH-pol) backscatter, the data set was limited to two nights and the use of visual inspection to confirm the presence of dew. Our inclusion of continuous LWSs allowed us to capture the accumulation, peak and dissipation of dew every night for the entire growing season, ensuring that our conclusions are based on a diverse range of events.

The inclusion of continuous leaf wetness measurements also provides unique, new insights into L-band backscatter sensitivity to rainfall interception. Light rain events, intercepted by the vegetation, caused strong fluctuations in σ^0 (3 dB in cross-pol and 2 dB in copol), even though soil moisture was constant [see Fig. 6(a)–(c)]. The presence of SCW is not considered in current electromagnetic models (e.g., [75], [86], [87]) or retrieval algorithms (e.g., [20], [79], [88]). The results presented here demonstrate that SCW can have a significant effect on σ^0. Accounting for SCW in models and retrieval algorithms can therefore be expected to lead to improved retrievals of soil and vegetation variables.

The significant effect of both dew and interception on σ^0 illustrates the value of including continuous LWSs in microwave field campaigns and experiments. In this study, SCW was estimated from LWS data using a simple weighting based on LAI. While this was sufficient to demonstrate the important influence that SCW has on the canopy, rigorous validation of SCW is essential in future experiments that seek to establish quantitative relationships between SCW and σ^0. Given that microwaves penetrate the vegetation, future research should also examine how the vertical distribution of SCW influences its effect on σ^0.

V. Conclusion

Results from an intensive experimental campaign combining subdaily radar and vegetation water dynamics observations were used to explore the sensitivity of L-band radar backscatter to variations in surface and internal canopy water content of corn. The daily cycle in radar backscatter was found to vary in amplitude depending on the growth stage of the vegetation. Though the strongest diurnal variations were observed during the early vegetative stages, the limited vegetation scattering and attenuation during this time suggests that these variations are attributed to surface soil moisture fluctuations and heavy dew on the uppermost skin of the soil. As the canopy approached full biomass, the sensitivity to the underlying soil was strongly reduced, and the diurnal cycle in radar backscatter was found to reflect temporal patterns in surface and internal water content.

Radar backscatter, especially in cross-pol, was found to be sensitive to SCW, with temporal variations in radar backscatter closely following the slow accumulation and rapid dissipation of dew, and exhibiting transient but significant increases in response to interception. In addition to being a variable of interest in its own right, the prevalence of dew during the night and early morning and its influence on the radar backscatter highlights the potential influence of overpass time on the interpretation of radar observations from sun-synchronous satellites for vegetation monitoring. It also highlights the potential benefit of being able to choose subdaily SAR data at specific overpass times to avoid the confounding influence of dew on the retrieval of biomass and internal water content. Both the effects of surface and internal canopy water on backscatter underscore the importance of including canopy water dynamics in physical models, particularly those used to simulate subdaily radar observations.

One of the key challenges of exploiting subdaily spaceborne SAR will be to disentangle surface and internal water content. Continuous monitoring of SCW significantly improved the interpretation of subdaily radar. During the daytime, interception events are often transient and easily identifiable, and dew dissipation is often rapid. However, the slower dynamics of dew accumulation and internal water content variations are more difficult to separate. Developing a reliable approach to monitor VWC continuously would ease this separation of signals, and would improve the interpretation of subdaily radar significantly. The sensitivity to surface and internal water content variations was found to be polarization-dependent. This suggests that subdaily polarimetric SAR (PolSAR) could be particularly useful to disentangle surface from internal canopy water variations.

The results demonstrate a potentially valuable application for subdaily spaceborne SAR missions. However, the data set is limited to a single crop type and a single radar configuration. There are many open questions to be addressed. Planned and candidate missions have been proposed that could yield data at different frequencies. Additional experimental research is essential to explore the sensitivity of backscatter from L-, to Ku-band to canopy water dynamics given the influence that frequency will have on both the penetration depth in the canopy and the sensitivity to the various vegetation constituents. The influence of viewing geometry also warrants investigation. The incidence angle of radar backscatter observations from geostationary satellites varies by latitude. Hence, the suitability of subdaily SAR data may be limited to certain latitudinal bands. For constellations, a time series of data for a given location on the ground will combine acquisitions that may vary by incidence and azimuth angle. Both influence backscatter, particularly in agricultural areas, so their impact on the relative sensitivity to surface and internal water content and soil moisture and roughness should be characterized. Moreover, given the importance of rainfall interception on the radar signals and its complexity, more research should be conducted on a better estimating interception, under different conditions, for different types and stages of vegetation, and the effect of the distribution of intercepted water in the canopy on backscatter.

The future availability of subdaily fine resolution data on surface and internal water content offers an extraordinary opportunity to study plant water dynamics from a new perspective, and at the landscape scales most relevant for understanding water and carbon exchanges in the climate system. By providing information on rapid surface and internal plant water dynamics, subdaily spaceborne SAR has the potential to become a valuable source of data in the fields of hydrology, land surface modeling, climate modeling, numerical weather prediction, and plant physiology.

APPENDIX
ELECTROMAGNETIC MODEL SIMULATIONS

A physical model for corn, developed at the Tor Vergata University of Rome [86], [89], was used to illustrate contributions of soil and vegetation components to total backscatter, and the changes during the season. This model is based on the radiative transfer theory and provides polarimetric backscatter of agricultural fields. It is able to simulate both scattering and extinction properties of vegetation elements and of the underlying soil applying the most suitable electromagnetic approximation, depending on the scatterer size and shape. Furthermore, it is able to take into account multiple scattering of any order and it can separate contributions of different scatterers in the vegetation canopy.

The inputs for the model are listed in Table III. Soil root mean square (rms) height was estimated using the meshboard approach described in [90], and was measured in the period between sowing and crop emergence. The correlation length is very difficult to measure accurately because it is extremely variable [91]. Therefore, we chose the correlation length which gave the best fit between simulated and observed σ^0 during the bare soil period. Plant density was averaged over 40 randomly chosen samples. The model was run with a daily time step. Because the model does not account for SCW, soil moisture values at 10:00 were used to ensure that dew had dissipated from the canopy at the observation time. Since water on leaves suppresses transpiration [10], the internal water content at 10:00 should be close to 6:00 observations. Time series of vegetation parameters were linearly interpolated. Similar to the observed σ^0, cross-polarized backscatter represents the average of VH and HV polarizations.

The model simulations (root mean square error (RMSE) = 3.91 dB) are presented in Fig. 10. Note that the observed copolarized backscatter is underestimated by the model, while the cross-pol increase due to vegetation growth is very well reproduced. *Vegetation* scattering refers to the volume scattering by the vegetation layer. *Ground* scattering refers to direct scattering solely from the ground. *Vegetation-ground* scattering represents multiple scattering effects due to interactions between the vegetation and ground. *Double-bounce* scattering represents the contribution coming from specular reflection from the soil followed by a specular reflection by stems, and vice versa.

Copolarized backscatter was dominated by the direct ground contribution in the early season. Increasing VWC during the vegetative stages (Fig. 2) results in attenuation of the ground contribution, and an increase in the vegetation, vegetation-ground, and double-bounce terms. Double-bounce scattering increases with stem growth and is most significant in VV during the early vegetative stages.

Both copolarized σ^0 simulations are dominated by direct vegetation scattering after May 16, when LAI $>$ 1, and VWC $>$ 1.5 kg m^{-2}. After May 23, when LAI $>$ 3.5 and VWC $>$ 3.5 kg m^{-2}, σ_{VV} simulations can be almost completely explained by direct scattering from vegetation in mid- and late season, and other scattering mechanisms

TABLE III
INPUT PARAMETERS FOR MODEL SIMULATION

Parameter	Single value or time series
Frequency	1.25 GHz
Incidence angle	40°
Soil rms height	2.5 cm
Soil correlation length	33 cm
Surface soil moisture (10:00)	Time series
Crop height	Time series
M_g cylinders (stems)	Time series
M_g discs (leaves)	Time series
No. of leaves	Time series
LAI	Time series
Stem height	Time series
Stem radius	Time series
Leaf area	Time series
Plant density	8 plants m^{-2}

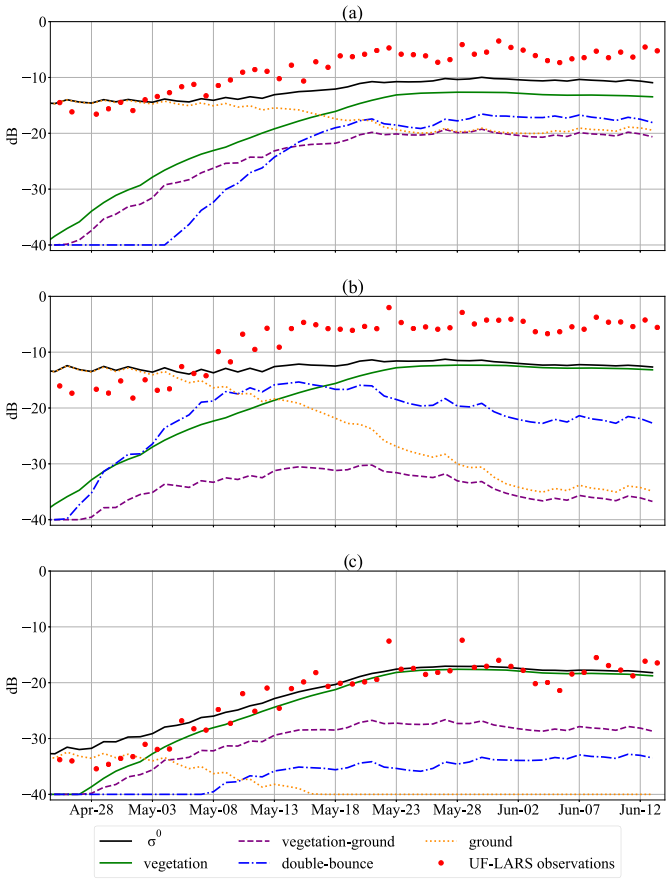

Fig. 10. Tor Vergata model simulations for (a) HH-polarized backscatter, (b) VV-polarized backscatter, and (c) cross-polarized backscatter. UF-LARS observations at 10:00 are plotted for reference.

are negligible. However, indirect and direct scattering from the ground still contributes to σ_{HH} to some degree in this period. These results are comparable to those of [78], where a larger double bounce effect at HH polarization is observed, due to a much smoother soil surface. Cross-polarized backscatter (σ_{cross}) was dominated by direct scattering from vegetation, even when the plants were still small.

ACKNOWLEDGMENT

The experiment was made possible by infrastructural and technical support from the Department of Agricultural and Biological Engineering and PSREU at the University of Florida. The authors would like to thank Daniel Preston and Patrick Rush for their technical support, Eduardo Carrascal for data collection and processing, James Boyer and his team for their on-farm logistical support, and Roger DeRoo for useful insights about the UF-LARS system. We also appreciate the efforts of the five anonymous reviewers and the editor.

REFERENCES

[1] J. B. Fisher *et al.*, "The future of evapotranspiration: Global requirements for ecosystem functioning, carbon and climate feedbacks, agricultural management, and water resources," *Water Resour. Res.*, vol. 53, no. 4, pp. 2618–2626, Apr. 2017.

[2] B. Mueller *et al.*, "Benchmark products for land evapotranspiration: LandFlux-EVAL multi-data set synthesis," *Hydrol. Earth Syst. Sci.*, vol. 17, no. 10, pp. 3707–3720, Oct. 2013.

[3] C. Jiménez *et al.*, "Global intercomparison of 12 land surface heat flux estimates," *J. Geophys. Res.*, vol. 116, no. D2, pp. 1–27, 2011.

[4] J. Mao *et al.*, "Disentangling climatic and anthropogenic controls on global terrestrial evapotranspiration trends," *Environ. Res. Lett.*, vol. 10, no. 9, Sep. 2015, Art. no. 094008.

[5] E. Blyth and R. J. Harding, "Methods to separate observed global evapotranspiration into the interception, transpiration and soil surface evaporation components," *Hydrol. Processes*, vol. 25, no. 26, pp. 4063–4068, Dec. 2011.

[6] S. T. Allen *et al.*, "Key questions on the evaporation and transport of intercepted precipitation," in *Precipitation Partitioning by Vegetation: A Global Synthesis*, J. Van Stan, II, E. Gutmann, and J. Friesen, Eds. Cham, Switzerland: Springer, 2020, pp. 269–280.

[7] A. I. J. M. van Dijk *et al.*, "Rainfall interception and the coupled surface water and energy balance," *Agricult. Forest Meteorol.*, vols. 214–215, pp. 402–415, Dec. 2015.

[8] S. M. de Jong and V. G. Jetten, "Estimating spatial patterns of rainfall interception from remotely sensed vegetation indices and spectral mixture analysis," *Int. J. Geograph. Inf. Sci.*, vol. 21, no. 5, pp. 529–545, May 2007.

[9] A. Klamerus-Iwan, T. E. Link, R. F. Keim, and J. T. Van Stan, II, "Storage and routing of precipitation through canopies," in *Precipitation Partitioning by Vegetation: A Global Synthesis*, J. I. Van Stan, E. Gutmann, and J. Friesen, Eds. Cham, Switzerland: Springer, 2020, pp. 17–34.

[10] T. E. Dawson and G. R. Goldsmith, "The value of wet leaves," *New Phytol.*, vol. 219, no. 4, pp. 1156–1169, Sep. 2018.

[11] C. Allen and F. Ulaby, "Modelling the polarization dependence of the attenuation in vegetation canopies," in *Proc. IGARSS Symp.*, Strasbourg, France, Aug. 1984, pp. 119–124.

[12] F. Ulaby and M. El-rayes, "Microwave dielectric spectrum of vegetation—Part II: Dual-dispersion model," *IEEE Trans. Geosci. Remote Sens.*, vol. GRS-25, no. 5, pp. 550–557, Sep. 1987.

[13] M. El-rayes and F. Ulaby, "Microwave dielectric spectrum of vegetation—Part I: Experimental observations," *IEEE Trans. Geosci. Remote Sens.*, vol. GRS-25, no. 5, pp. 541–549, Sep. 1987.

[14] F. Ulaby, "Radar response to vegetation," *IEEE Trans. Antennas Propag.*, vol. AP-23, no. 1, pp. 36–45, Jan. 1975.

[15] F. Ulaby, T. Bush, and P. Batlivala, "Radar response to vegetation II: 8-18 GHz band," *IEEE Trans. Antennas Propag.*, vol. AP-23, no. 5, pp. 608–618, Sep. 1975.

[16] B. Brisco, R. Brown, J. Koehler, G. Sofko, and M. Mckibben, "The diurnal pattern of microwave backscattering by wheat," *Remote Sens. Environ.*, vol. 34, no. 1, pp. 37–47, Oct. 1990.

[17] T. Gillespie, B. Brisco, R. Brown, and G. Sofko, "Radar detection of a dew event in wheat," *Remote Sens. Environ.*, vol. 33, no. 3, pp. 151–156, Sep. 1990.

[18] F. T. Ulaby, A. Aslam, and M. C. Dobson, "Effects of vegetation cover on the radar sensitivity to soil moisture," *IEEE Trans. Geosci. Remote Sens.*, vol. GRS-20, no. 4, pp. 476–481, Oct. 1982.

[19] P. E. O'Neill, N. S. Chauhan, and T. J. Jackson, "Use of active and passive microwave remote sensing for soil moisture estimation through corn," *Int. J. Remote Sens.*, vol. 17, no. 10, pp. 1851–1865, Jul. 1996.

[20] A. T. Joseph, R. van der Velde, P. E. O'Neill, R. H. Lang, and T. Gish, "Soil moisture retrieval during a corn growth cycle using L-band (1.6 GHz) radar observations," *IEEE Trans. Geosci. Remote Sens.*, vol. 46, no. 8, pp. 2365–2374, Aug. 2008.

[21] S. Quegan *et al.*, "The European space agency BIOMASS mission: Measuring forest above-ground biomass from space," *Remote Sens. Environ.*, vol. 227, pp. 44–60, Jun. 2019.

[22] J. Reiche, E. Hamunyela, J. Verbesselt, D. Hoekman, and M. Herold, "Improving near-real time deforestation monitoring in tropical dry forests by combining dense Sentinel-1 time series with Landsat and ALOS-2 PALSAR-2," *Remote Sens. Environ.*, vol. 204, pp. 147–161, Jan. 2018.

[23] A. G. Konings, K. Rao, and S. C. Steele-Dunne, "Macro to micro: Microwave remote sensing of plant water content for physiology and ecology," *New Phytol.*, vol. 223, no. 3, pp. 1166–1172, 2019, doi: 10.1111/nph.15808.

[24] S. C. Steele-Dunne, H. McNairn, A. Monsivais-Huertero, J. Judge, P.-W. Liu, and K. Papathanassiou, "Radar remote sensing of agricultural canopies: A review," *IEEE J. Sel. Topics Appl. Earth Observ. Remote Sens.*, vol. 10, no. 5, pp. 2249–2273, May 2017.

[25] R. Torres *et al.*, "GMES Sentinel-1 mission," *Remote Sens. Environ.*, vol. 120, pp. 9–24, May 2012.

[26] G. Satalino *et al.*, "Sentinel-1 & Sentinel-2 data for soil tillage change detection," in *Proc. IEEE Int. Geosci. Remote Sens. Symp. (IGARSS)*, Valencia, Spain, Jul. 2018, pp. 6627–6630.

[27] A. Veloso *et al.*, "Understanding the temporal behavior of crops using Sentinel-1 and Sentinel-2-like data for agricultural applications," *Remote Sens. Environ.*, vol. 199, pp. 415–426, Sep. 2017.

[28] S. Khabbazan *et al.*, "Crop monitoring using Sentinel-1 data: A case study from The Netherlands," *Remote Sens.*, vol. 11, no. 16, p. 1887, Aug. 2019.

[29] M. El Hajj *et al.*, "First vegetation optical depth mapping from sentinel-1 C-band SAR data over crop fields," *Remote Sens.*, vol. 11, no. 23, p. 2769, Jan. 2019.

[30] M. Vreugdenhil *et al.*, "Sensitivity of Sentinel-1 backscatter to vegetation dynamics: An Austrian case study," *Remote Sens.*, vol. 10, no. 9, p. 1396, Sep. 2018.

[31] A. Mercier *et al.*, "Evaluation of Sentinel-1 & 2 time series for predicting wheat and rapeseed phenological stages," *ISPRS J. Photogramm. Remote Sens.*, vol. 163, pp. 231–256, May 2020.

[32] Mahdianpari *et al.*, "Mid-season crop classification using dual-, compact-, and full-polarization in preparation for the radarsat constellation mission (RCM)," *Remote Sens.*, vol. 11, no. 13, p. 1582, Jul. 2019.

[33] *Capella Space*. Accessed: Mar. 19, 2020. [Online]. Available: http://www.capellaspace.com

[34] *ICEYE*. Accessed: Mar. 19, 2020. [Online]. Available: http://www.iceye.com

[35] C. Stringham *et al.*, "The capella X-band SAR constellation for rapid imaging," in *Proc. IEEE Int. Geosci. Remote Sens. Symp. (IGARSS)*, Jul. 2019, pp. 9248–9251.

[36] S. E. Hobbs *et al.*, "G-CLASS: Geosynchronous radar for water cycle science—Orbit selection and system design," *J. Eng.*, vol. 2019, no. 21, pp. 7534–7537, Nov. 2019.

[37] C. Hu, Y. Li, X. Dong, C. Cui, and T. Long, "Impacts of temporal-spatial variant background ionosphere on repeat-track GEO D-InSAR system," *Remote Sens.*, vol. 8, no. 11, p. 916, Nov. 2016.

[38] J. Matar, M. Rodriguez-Cassola, G. Krieger, P. Lopez-Dekker, and A. Moreira, "MEO SAR: System concepts and analysis," *IEEE Trans. Geosci. Remote Sens.*, vol. 58, no. 2, pp. 1313–1324, Feb. 2020.

[39] A. G. Konings, Y. Yu, L. Xu, Y. Yang, D. S. Schimel, and S. S. Saatchi, "Active microwave observations of diurnal and seasonal variations of canopy water content across the humid african tropical forests," *Geophys. Res. Lett.*, vol. 44, no. 5, pp. 2290–2299, Mar. 2017.

[40] A. C. Paget, D. G. Long, and N. M. Madsen, "RapidScat diurnal cycles over land," *IEEE Trans. Geosci. Remote Sens.*, vol. 54, no. 6, pp. 3336–3344, Jun. 2016.

[41] T. van Emmerik *et al.*, "Water stress detection in the Amazon using radar," *Geophys. Res. Lett.*, vol. 44, no. 13, pp. 6841–6849, Jul. 2017.

[42] S. Frolking, T. Milliman, M. Palace, D. Wisser, R. Lammers, and M. Fahnestock, "Tropical forest backscatter anomaly evident in SeaWinds scatterometer morning overpass data during 2005 drought in Amazonia," *Remote Sens. Environ.*, vol. 115, no. 3, pp. 897–907, Mar. 2011.

[43] R. Schroeder, K. C. McDonald, M. Azarderakhsh, and R. Zimmermann, "ASCAT MetOp-A diurnal backscatter observations of recent vegetation drought patterns over the contiguous U.S.: An assessment of spatial extent and relationship with precipitation and crop yield," *Remote Sens. Environ.*, vol. 177, pp. 153–159, May 2016.

[44] J. Friesen, S. C. Steele-Dunne, and N. van de Giesen, "Diurnal differences in global ERS scatterometer backscatter observations of the land surface," *IEEE Trans. Geosci. Remote Sens.*, vol. 50, no. 7, pp. 2595–2602, Jul. 2012.

[45] S. C. Steele-Dunne, S. Hahn, W. Wagner, and M. Vreugdenhil, "Investigating vegetation water dynamics and drought using metop ASCAT over the North American grasslands," *Remote Sens. Environ.*, vol. 224, pp. 219–235, Apr. 2019.

[46] F. Ulaby and P. Batlivala, "Diurnal variations of radar backscatter from a vegetation canopy," *IEEE Trans. Antennas Propag.*, vol. 24, no. 1, pp. 11–17, Jan. 1976.

[47] W. Bouten, P. J. F. Swart, and E. De Water, "Microwave transmission, a new tool in forest hydrological research," *J. Hydrol.*, vol. 124, no. 1, pp. 119–130, Apr. 1991.

[48] J. J. M. de Jong, W. Klaassen, and P. J. C. Kuiper, "Monitoring of rain water storage in forests with satellite radar," *IEEE Trans. Geosci. Remote Sens.*, vol. 40, no. 2, pp. 338–347, Feb. 2002.

[49] K. C. Mcdonald, M. C. Dobson, and F. T. Ulaby, "Using mimics to model L-band multiangle and multitemporal backscatter from a walnut orchard," *IEEE Trans. Geosci. Remote Sens.*, vol. 28, no. 4, pp. 477–491, Jul. 1990.

[50] J. Weber and S. Ustin, "Diurnal water relations of walnut trees: Implications for remote sensing," *IEEE Trans. Geosci. Remote Sens.*, vol. 29, no. 6, pp. 864–874, Nov. 1991.

[51] K. C. McDonald, R. Zimmerman, and J. Way, "An investigation of the relationship between tree water potential and dielectric constant," in *Proc. Int. Geosci. Remote Sens. Symp. (IGARSS)*, May 1992, pp. 523–525.

[52] W. A. Salas, J. K. Ranson, B. N. Rock, and K. T. Smith, "Temporal and spatial variations in dielectric constant and water status of dominant forest species from New England," *Remote Sens. Environ.*, vol. 47, no. 2, pp. 109–119, Feb. 1994.

[53] R. Zimmermann, K. McDonald, R. Oren, and J. Way, "Xylem dielectric constant, water status, and transpiration of young Jack Pine (Pinus banksiana Lamb.) in the southern boreal zone of Canada," in *Proc. IGARSS*, vol. 2, Jul. 1995, pp. 1006–1008.

[54] K. C. McDonald, R. Zimmermann, and J. S. Kimball, "Diurnal and spatial variation of xylem dielectric constant in Norway spruce (Picea abies [L.] Karst.) as related to microclimate, xylem sap flow, and xylem chemistry," *IEEE Trans. Geosci. Remote Sens.*, vol. 40, no. 9, pp. 2063–2082, Sep. 2002.

[55] T. Bongiovanni *et al.*, "Field Observations during the tenth microwave water and energy balance experiment (MicroWEX-10): From March 1, 2011, through January 5, 2012," Dept. Agricult. Biol. Eng., Univ. Florida, Inst. Food Agricult. Sci., Gainesville, FL, USA, Tech. Rep. AE514, 2015.

[56] M. Bongiovanni *et al.*, "Field observations during the eleventh microwave water and energy balance experiment (MicroWEX-11): From April 25, 2012, through December 6, 2012," Dept. Agricult. Biol. Eng., Univ. Florida, Inst. Food Agricult. Sci., Gainesville, FL, USA, Tech. Rep. AE512, 2018.

[57] K. Nagarajan *et al.*, "Automated L-band radar system for sensing soil moisture at high temporal resolution," *IEEE Geosci. Remote Sens. Lett.*, vol. 11, no. 2, pp. 504–508, Feb. 2014.

[58] K. Sarabandi and F. T. Ulaby, "A convenient technique for polarimetric calibration of single-antenna radar systems," *IEEE Trans. Geosci. Remote Sens.*, vol. 28, no. 6, pp. 1022–1033, Nov. 1990.

[59] P.-W. Liu, "Integration of active and passive microwave signatures for characterization of soil properties," Ph.D. dissertation, Dept. Agricult. Biol. Eng., Univ. Florida, Gainesville, FL, USA, 2013.

[60] P.-W. Liu, J. Judge, R. D. DeRoo, A. W. England, T. Bongiovanni, and A. Luke, "Dominant backscattering mechanisms at L-band during dynamic soil moisture conditions for sandy soils," *Remote Sens. Environ.*, vol. 178, pp. 104–112, Jun. 2016.

[61] L. Zotarelli, M. D. Dukes, C. C. Romero, and K. W. Migliaccio, "Step by step calculation of the Penman-Monteith evapotranspiration (FAO-56 method)," Dept. Agricult. Biol. Eng., Univ. Florida, Inst. Food Agricult. Sci., Gainesville, FL, USA, Tech. Rep. AE459, 2018.

[62] J. Cermak, J. Kucera, W. L. Bauerle, N. Phillips, and T. M. Hinckley, "Tree water storage and its diurnal dynamics related to sap flow and changes in stem volume in old-growth douglas-fir trees," *Tree Physiol.*, vol. 27, no. 2, pp. 181–198, Feb. 2007.

[63] F. C. Meinzer, S. A. James, and G. Goldstein, "Dynamics of transpiration, sap flow and use of stored water in tropical forest canopy trees," *Tree Physiol.*, vol. 24, no. 8, pp. 901–909, Aug. 2004.

[64] N. G. Phillips, F. G. Scholz, S. J. Bucci, G. Goldstein, and F. C. Meinzer, "Using branch and basal trunk sap flow measurements to estimate whole-plant water capacitance: Comment on Burgess and Dawson (2008)," *Plant Soil*, vol. 315, pp. 315–324, Aug. 2008.

[65] T. Sakuratani, "A heat balance method for measuring water flux in the stem of intact plants," *J. Agricult. Meteorol.*, vol. 37, no. 1, pp. 9–17, 1981.

[66] J. M. Baker and C. H. M. Bavel, "Measurement of mass flow of water in the stems of herbaceous plants," *Plant, Cell Environ.*, vol. 10, no. 9, pp. 777–782, Dec. 1987.

[67] *Dynagage Installation and Operation Manual*, Dynamax, Houston, TX, USA, 2007.

[68] M. G. van Bavel, J. S. Young, and L. H. Comas, "Installation and validation of sap flow sensors on maize plants," Dynamax Inc., Houston, TX, USA, Tech. Rep., Jul. 2016.

[69] *Crop Evapotranspiration: Guidelines for Computing Crop Water Requirements*, FAO Irrigation Drainage, Rome, Italy, 1998.

[70] *PHYTOS 31, Dielectric Leaf Wetness Sensor, Product Manual*, Meter Group, Inc., Pullman, WA, USA, 2019.

[71] D. Cobos, "Predicting the amount of water on the surface of the LWS dielectric leaf wetness sensor," Decagon Devices, Inc., Pullman, WA, USA, Appl. Note 14556-01, 2013.

[72] *T4/T4e Pressure Transducer Tensiometer, User Manual*, UMS GmbH, München, Germany, Dec. 2011.

[73] D. Entekhabi *et al.*, "The soil moisture active passive (SMAP) mission," *Proc. IEEE*, vol. 98, no. 5, pp. 704–716, May 2010.

[74] W. Meier *et al.*, "The BBCH system to coding the phenological growth stages of plants—History—Publications," *J. für Kulturpflanzen*, vol. 61, no. 2, pp. 41–52, 2009.

[75] A. Monsivais-Huertero, P.-W. Liu, and J. Judge, "Phenology-based backscattering model for corn at L-band," *IEEE Trans. Geosci. Remote Sens.*, vol. 56, no. 9, pp. 4989–5005, Sep. 2018.

[76] H. McNairn, J. Shang, X. Jiao, and C. Champagne, "The contribution of ALOS PALSAR multipolarization and polarimetric data to crop classification," *IEEE Trans. Geosci. Remote Sens.*, vol. 47, no. 12, pp. 3981–3992, Dec. 2009.

[77] H. Joerg, "Multi-frequency polarimetric SAR tomography for the 3-D characterization and monitoring of agricultural crops," Ph.D. dissertation, Dept. Civil, Environ. Geomatic Eng., ETH Zurich, Zürich, Switzerland, 2018.

[78] J. Stamenkovic, P. Ferrazzoli, L. Guerriero, D. Tuia, and J.-P. Thiran, "Joining a discrete radiative transfer model and a kernel retrieval algorithm for soil moisture estimation from SAR data," *IEEE J. Sel. Topics Appl. Earth Observ. Remote Sens.*, vol. 8, no. 7, pp. 3463–3475, Jul. 2015.

[79] P. C. Dubois, J. van Zyl, and T. Engman, "Measuring soil moisture with imaging radars," *IEEE Trans. Geosci. Remote Sens.*, vol. 33, no. 4, pp. 915–926, Jul. 1995.

[80] S. Paloscia, G. Macelloni, P. Pampaloni, and S. Sigismondi, "The potential of C- and L-band SAR in estimating vegetation biomass: The ERS-1 and JERS-1 experiments," *IEEE Trans. Geosci. Remote Sens.*, vol. 37, no. 4, pp. 2107–2110, Jul. 1999.

[81] T.-H. Liao, S.-B. Kim, S. Tan, L. Tsang, C. Su, and T. J. Jackson, "Multiple scattering effects with cyclical correction in active remote sensing of vegetated surface using vector radiative transfer theory," *IEEE J. Sel. Topics Appl. Earth Observ. Remote Sens.*, vol. 9, no. 4, pp. 1414–1429, Apr. 2016.

[82] S. C. Steele-Dunne, J. Friesen, and N. van de Giesen, "Using diurnal variation in backscatter to detect vegetation water stress," *IEEE Trans. Geosci. Remote Sens.*, vol. 50, no. 7, pp. 2618–2629, Jul. 2012.

[83] M. Herold, C. Pathe, and C. Schmullius, "The effect of free vegetation water on the multi-frequency and polarimetric radar backscatter-first, results from the Terradew 2000 campaign," in *Proc. Scanning Present Resolving Future IEEE Int. Geosci. Remote Sens. Symp.*, Sydney, NSW, Australia, vol. 5, Jul. 2001, pp. 2445–2447.

[84] D. Wood, H. McNairn, R. J. Brown, and R. Dixon, "The effect of dew on the use of RADARSAT-1 for crop monitoring: Choosing between ascending and descending orbits," *Remote Sens. Environ.*, vol. 80, no. 2, pp. 241–247, May 2002.
[85] B. K. Hornbuckle *et al.*, "Howdoes dew affect L-band backscatter? Analysis of pals data at the iowa validation site and implications for SMAP," in *Proc. IEEE Int. Geosci. Remote Sens. Symp.*, Jul. 2010, pp. 4835–4838.
[86] M. Bracaglia, P. Ferrazzoli, and L. Guerriero, "A fully polarimetric multiple scattering model for crops," *Remote Sens. Environ.*, vol. 54, no. 3, pp. 170–179, Dec. 1995.
[87] F. Ulaby, K. Sarabandi, K. McDonald, M. Whitt, and M. Dobson, "Michigan microwave canopy scattering model. international journal of remote sensing," *Int. J. Remote Sens.*, vol. 11, no. 7, pp. 1223–1253, 1990.
[88] M. Hosseini, H. McNairn, A. Merzouki, and A. Pacheco, "Estimation of leaf area index (LAI) in corn and soybeans using multi-polarization C- and L-band radar data," *Remote Sens. Environ.*, vol. 170, pp. 77–89, Dec. 2015.
[89] A. Della Vecchia *et al.*, "Influence of geometrical factors on crop backscattering at C-band," *IEEE Trans. Geosci. Remote Sens.*, vol. 44, no. 4, pp. 778–790, Apr. 2006.
[90] M.-Y. Jang, K.-J. C. Tien, J. Casanova, and J. Judge, "Measurements of soil surface roughness during the fourth microwave water and energy balance experiment: April 18 through June 13, 2005," Dept. Agricult. Biol. Eng., Univ. Florida, Inst. Food Agricult. Sci., Gainesville, FL, USA, Tech. Rep. CIR1483, 2005.
[91] J. Álvarez-Mozos, M. González-Audícana, J. Casalí, and A. Larrañaga, "Effective versus measured correlation length for radar-based surface soil moisture retrieval," *Int. J. Remote Sens.*, vol. 29, nos. 17–18, pp. 5397–5408, Sep. 2008.

Paul C. Vermunt received the B.Sc. degree in environmental sciences and the M.Sc. degree in hydrology from Utrecht University, Utrecht, The Netherlands, in 2013 and 2016, respectively. He is pursuing the Ph.D. degree with the Department of Water Management, Faculty of Civil Engineering and Geosciences, Delft University of Technology, Delft, The Netherlands.

His main research interest includes applying radar to monitor vegetation water dynamics.

Saeed Khabbazan received the B.Sc. degree in surveying and geomatics engineering from Tabriz University, Tabriz, Iran, in 2011, and the M.Sc. degree in remote sensing from Tehran University, Tehran, Iran, in 2014. He is pursuing the Ph.D. degree with the Department of Water Management, Faculty of Civil Engineering and Geosciences, Delft University of Technology, Delft, The Netherlands.

His research interest includes remote sensing over land using active microwave instruments.

Susan C. Steele-Dunne (Member, IEEE) received the S.M. and Ph.D. degrees in hydrology from the Massachusetts Institute of Technology, Cambridge, MA, USA, in 2002 and 2006, respectively.

She has been with the Faculty of Civil Engineering and Geosciences, Delft University of Technology, Delft, The Netherlands since 2008. She leads the M-WAVE Group, Nonthaburi, Thailand, who perform research from field to global scales, combining *in situ* and spaceborne sensors to improve our understanding of microwave interactions with vegetation. Her research interests include the use of data assimilation, modeling and machine learning to exploit spaceborne radar instruments for applications in ecosystem and agricultural monitoring.

Jasmeet Judge (Senior Member, IEEE) received the Ph.D. degree in electrical engineering and atmospheric, oceanic, and space sciences from the University of Michigan, Ann Arbor, MI, USA, in 1999.

She is a Professor with the Department of Agricultural and Biological Engineering, Institute of Food and Agricultural Sciences, University of Florida, Gainesville, FL, USA, where she is also the Director of the Center for Remote Sensing. Her research interests include microwave remote-sensing applications to terrestrial hydrology for dynamic vegetation, modeling of energy and moisture interactions at the land surface and in the vadose zone, spatio-temporal scaling of remotely sensed observations in heterogeneous landscapes; and data assimilation.

Alejandro Monsivais-Huertero (Senior Member, IEEE) received the B.S. degree in telecommunications engineering from the National Autonomous University of Mexico, Mexico City, Mexico, in 2002, and the M.S. degree in microwaves and optical telecommunications and the Ph.D. degree in microwaves, electromagnetism, and optoelectronics from the University of Toulouse, Toulouse, France, in 2004 and 2007, respectively.

From 2004 to 2006, he was with the Antennes, Dispositifs et Matériaux Microondes Laboratory, University of Toulouse. From 2006 to 2007 he was with the Laboratoire d'Etudes et de Recherche en Imagerie Spatiale et Médicale, University of Toulouse. From 2008 to 2009, he was a Postdoctoral Research Associate with the Department of Agricultural and Biological Engineering, Center for Remote Sensing, University of Florida, Gainesville, FL, USA. Since 2010, he has been working as a Researcher with the Superior School of Mechanical and Electrical Engineering, Ticoman Campus, National Polytechnic Institute of Mexico, Mexico City. His research areas of interest are in microwave and millimeter-wave radar remote sensing, electromagnetic wave propagation, and retrieval algorithms.

Leila Guerriero (Member, IEEE) received the Laurea degree in physics from Sapienza University of Rome, Rome, Italy, in 1986, and the Ph.D. degree in electromagnetism from the Tor Vergata University of Rome, Rome, in 1991.

Since 1994, she has been a Permanent Researcher with Tor Vergata University, where she is an Associate Professor holding the courses on Earth Satellite Observation and on Geoinformation. Her research interests include modeling microwave scattering and emissivity from agricultural and forested areas. She participated in several international projects, among them: the European Space Agency (ESA) Projects Soil Moisture and Ocean Salinity Satellite, Development of SAR Inversion Algorithms for Land Applications, Use of Bistatic Microwave Measurements for Earth Observation, and SAR Observation and Communications Satellite-Companion Satellite (SAOCOM-CS) Bistatic Imaging, Radiometry and Interferometry Over Land. Lately. She has been involved in the modeling of Global Navigation Satellite System Reflectometry (GNSS-R) signals for ESA Projects and in the European FP7 and H2020 Programs.

Dr. Guerriero is a member of the Permanent Steering Scientific Committee of MicroRad. She is the Secretary of the Geoscience and Remote Sensing Society (GRSS) North-Central Italy Chapter.

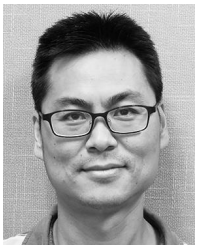

Pang-Wei Liu (Member, IEEE) received the Ph.D. degree in agricultural engineering with a minor in electrical engineering from the University of Florida, Gainesville, FL, USA, in 2013.

He is a Research Scientist with Hydrological Science Laboratory, NASA's Goddard Space Flight Center, Greenbelt, MD, USA, contracted through Science Systems and Applications, Inc., Lanham, MD USA. His research interests include active and passive microwave remote sensing modeling for soil moisture and agricultural crops, data disaggregation, groundwater monitoring using GRACE, data assimilation with crop growth models and land information system; application of light detection and ranging (LiDAR) for forest biomass, and GNSS-R remote sensing for terrestrial applications.

Dr. Liu is a member of the IEEE-Geoscience and Remote Sensing Society (GRSS) and the American Geophysical Union.